



HAL
open science

AGN-driven quenching of star formation: morphological and dynamical implications for early-type galaxies

Yohan Dubois, Raphaël Gavazzi, Sébastien Peirani, Joseph Silk

► **To cite this version:**

Yohan Dubois, Raphaël Gavazzi, Sébastien Peirani, Joseph Silk. AGN-driven quenching of star formation: morphological and dynamical implications for early-type galaxies. *Monthly Notices of the Royal Astronomical Society*, 2013, 433, pp.3297-3313. 10.1093/mnras/stt997 . hal-03645498

HAL Id: hal-03645498

<https://hal.science/hal-03645498v1>

Submitted on 23 Aug 2022

HAL is a multi-disciplinary open access archive for the deposit and dissemination of scientific research documents, whether they are published or not. The documents may come from teaching and research institutions in France or abroad, or from public or private research centers.

L'archive ouverte pluridisciplinaire **HAL**, est destinée au dépôt et à la diffusion de documents scientifiques de niveau recherche, publiés ou non, émanant des établissements d'enseignement et de recherche français ou étrangers, des laboratoires publics ou privés.

AGN-driven quenching of star formation: morphological and dynamical implications for early-type galaxies

Yohan Dubois,^{1,2*} Raphaël Gavazzi,¹ Sébastien Peirani¹ and Joseph Silk^{1,2,3}

¹*Institut d'Astrophysique de Paris, UMR 7095, CNRS, UPMC Univ. Paris VI, 98 bis boulevard Arago, F-75014 Paris, France*

²*Sub-department of Astrophysics, University of Oxford, Keble Road, Oxford OX1 3RH, UK*

³*Department of Physics and Astronomy, The Johns Hopkins University Homewood Campus, Baltimore, MD 21218, USA*

Accepted 2013 June 1. Received 2013 April 24; in original form 2013 January 14

ABSTRACT

In order to understand the physical mechanisms at work during the formation of massive early-type galaxies, we performed six zoomed hydrodynamical cosmological simulations of haloes in the mass range $4.3 \times 10^{12} \leq M_{\text{vir}} \leq 8.0 \times 10^{13} M_{\odot}$ at $z = 0$, using the Adaptive Mesh Refinement code `RAMSES`. These simulations explore the role of active galactic nuclei (AGN), through jets powered by the accretion on to supermassive black holes on the formation of massive elliptical galaxies. In the absence of AGN feedback, large amounts of stars accumulate in the central galaxies to form overly massive, blue, compact and rotation-dominated galaxies. Powerful AGN jets transform the central galaxies into red extended and dispersion-dominated galaxies. This morphological transformation of disc galaxies into elliptical galaxies is driven by the efficient quenching of the in situ star formation due to AGN feedback, which transform these galaxies into systems built up by accretion. For galaxies mainly formed by accretion, the proportion of stars deposited farther away from the centre increases, and galaxies have larger sizes. The accretion is also directly responsible for randomizing the stellar orbits, increasing the amount of dispersion over rotation of stars as a function of time. Finally, we find that our galaxies simulated with AGN feedback better match the observed scaling laws, such as the size–mass, velocity dispersion–mass, Fundamental Plane relations and slope of the total density profiles at $z \sim 0$, from dynamical and strong lensing constraints.

Key words: methods: numerical – galaxies: active – galaxies: elliptical and lenticular, cD – galaxies: formation – galaxies: jets – galaxies: kinematics and dynamics.

1 INTRODUCTION

Early-type galaxies (ETG) are amongst the most massive galaxies observed in our Universe. They are red, almost dead, and ellipsoidal-shaped objects lying in the densest regions of the Universe at redshift zero, predominately in groups and clusters of galaxies.

In the standard Λ cold dark matter (Λ CDM) paradigm, progenitors of massive collapsed structures such as groups and clusters of galaxies form at high redshift by the accretion of cold filamentary gas. At low redshift, the gas cooling rate at the virial radius becomes insufficient to efficiently evacuate the energy of infall transformed into heat due to shocks, and leads to the formation of large, diffuse and hot quasi-spherical regions of gas around bright galaxies (Rees & Ostriker 1977; White & Frenk 1991; Birnboim & Dekel 2003; Kereš et al. 2005; Ocvirk, Pichon & Teyssier 2008; Dekel et al. 2009a; van de Voort et al. 2011). However, in the absence of any strong source of feedback from galaxies, theory fails to produce

this population of red massive galaxies (e.g. Bower et al. 2006), as the gas cooling flows proceed uninterrupted in the cores of haloes. This leads to overly massive and actively star-forming galaxies at redshift zero, in stark contradiction with observations.

Supermassive black holes (BHs) are commonly observed in the centres of galaxies with bulges. The BH mass M_{BH} scales with its host bulge stellar mass M_{b} , and stellar velocity dispersion σ_{b} (Magorrian et al. 1998; Tremaine et al. 2002; Häring & Rix 2004; Gültekin et al. 2009; Graham & Scott 2013). This has led several authors to suggest that a self-regulation process is taking place between BHs and their host galaxy (Silk & Rees 1998; King 2003; Wyithe & Loeb 2003), as accretion on to supermassive BHs can release tremendous amounts of energy that can potentially drive large-scale outflows, and quench the star formation. This mechanism is also supported by the detection of strong active galactic nuclei (AGN) activity in groups and clusters in the form of radio jets (e.g. Boehringer et al. 1993), or in the distant Universe as seen through quasar spectra (e.g. Chartas, Brandt & Gallagher 2003).

Semi-analytical models of galaxy formation using cosmological N -body simulations have demonstrated that AGN feedback can

*E-mail: dubois@iap.fr

be responsible for creating a population of red and dead massive galaxies (Bower et al. 2006; Cattaneo et al. 2006; Croton et al. 2006; Somerville et al. 2008). Hydrodynamical cosmological simulations which are dynamically and spatially resolved where AGN feedback sub-grid prescriptions are implemented also confirm that this mechanism is able to self-regulate the baryon content in massive haloes to get realistic galaxy masses and colours (Sijacki & Springel 2006; Puchwein, Sijacki & Springel 2008; Khalatyan et al. 2008; McCarthy et al. 2010, 2011; Dubois et al. 2010, 2011; Teyssier et al. 2011), and that it can reproduce the relatively tight $M_{\text{BH}}-M_{\text{b}}$, $M_{\text{BH}}-\sigma_{\text{b}}$ relationships (Sijacki et al. 2007; Di Matteo et al. 2008; Booth & Schaye 2009; Dubois et al. 2012).

Studies of strong gravitational lensing by massive ETGs at low redshift ($z \sim 0.2$) have provided a wealth of information about their mass distribution thanks to sizeable sample of lenses that have been built up in the last few years. The most noticeable result from the Sloan Lens ACS (SLACS) survey (e.g. Koopmans et al. 2009; Auger et al. 2010a) is that the density profile within one half of the projected effective radius is found to be close to isothermal ($\rho \propto r^{-2}$) with little (~ 10 per cent) scatter around this value (see also Rusin, Kochanek & Keeton 2003). It is noteworthy to mention that these conclusions given by strong lenses apply to low ($z \sim 0.2$) redshift ETGs since most of this work builds on the Sloan Digital Sky Survey (SDSS). More recent results have suggested that the isothermal profile is also present at higher redshift ($z \sim 0.5$) but flatter than at low redshift (Ruff et al. 2011; Bolton et al. 2012).

Deep observations of distant galaxies have revealed that massive galaxies were more compact in the past (Daddi et al. 2005; Trujillo et al. 2006) than they are today. These observations challenge the scenario where galaxies are built from a monolithic collapse, and favour a scenario where mergers drive the formation of massive ETGs at $z = 0$. The size increase of these objects due to mergers is expected in semi-analytical theory and in numerical simulations (Boylan-Kolchin, Ma & Quataert 2006; Khochfar & Silk 2006b; Maller et al. 2006; Naab, Khochfar & Burkert 2006; Bournaud, Jog & Combes 2007; De Lucia & Blaizot 2007; Naab et al. 2007; Guo & White 2008; Hopkins et al. 2009; Nipoti et al. 2009; Feldmann et al. 2010; Shankar et al. 2013), and is supported by the direct evidence of merger remnants of what are the progenitors of today's most massive galaxies. Major mergers have been proposed as a solution for the evolution of the sizes of galaxies (e.g. Khochfar & Silk 2006a); however they are rare events (one major merger on average since $z = 2$) that cannot explain the rapid size–mass evolution with redshift (e.g. Bundy et al. 2009). Dry minor mergers seem to be appropriate candidates for growing the galaxy sizes as fast as found in the observations (Naab, Johansson & Ostriker 2009; Lackner & Ostriker 2010; Oser et al. 2010, 2012; Hilz et al. 2012).

Hydrodynamical cosmological simulations following the formation of elliptical galaxies by Oser et al. (2010), using smoothed particle hydrodynamics (SPH), have shown that these galaxies can be formed even in the absence of AGN feedback, because the fraction of accreted stellar mass dominates the fraction of in situ formed stars for low-redshift massive galaxies. This result has been challenged recently by Lackner et al. (2012), using Adaptive Mesh Refinement (AMR), where they find that in the absence of AGN feedback, in situ star formation dominates at all times, even at $z = 0$. The aim of this paper is to probe the role of AGN feedback on galaxy morphology, and on the history of mass accretion on to galaxies.

The paper is organized as follow. In Section 2, we describe our numerical model for galaxy formation and our zoom initial conditions. In Section 3, we detail the results obtained with our simulated

galaxies and the particular role of AGN feedback on the mass build-up of massive ETGs, and we check the consistency of dynamical properties with observations. In Section 4, we compare our work to previous numerical studies solving for gas hydrodynamics. Finally, in Section 5, we summarize the main results of this work and discuss the possible implications.

2 SIMULATION SET-UP

2.1 Initial conditions and simulation parameters

We assume a flat Λ CDM cosmology with total matter (baryons+DM) density $\Omega_{\text{m}} = 0.272$, baryon density $\Omega_{\text{b}} = 0.045$, dark energy density $\Omega_{\Lambda} = 0.728$, fluctuation amplitude at $8 h^{-1}$ Mpc $\sigma_8 = 0.809$ and Hubble constant $H_0 = 70.4 \text{ km s}^{-1} \text{ Mpc}^{-1}$ consistent with *Wilkinson Microwave Anisotropy Probe* 7-year data (Komatsu et al. 2011).

The simulations are run with the AMR code *RAMSES* (Teyssier 2002). The evolution of the gas is followed using a second-order unsplit Godunov scheme for the Euler equations. The Riemann solver used to compute the flux at the cell interface is the Harten-Lax-van Leer-Contact (HLLC) solver (Toro, Spruce & Speares 1994) and a first-order MinMod Total Variation Diminishing scheme is applied to reconstruct the interpolated variables from their cell-centred values. Collisionless particles (DM, stellar and sink particles) are evolved using a particle-mesh solver with a Cloud-In-Cell interpolation.

Two different box sizes $L_{\text{box}} = 100 h^{-1} \text{ Mpc}$ and $50 h^{-1} \text{ Mpc}$ have been used to generate the initial conditions. Six groups of galaxies in the mass range $4.3 \times 10^{12} \leq M_{\text{vir}} \leq 8.0 \times 10^{13} M_{\odot}$ have been selected to be resimulated at high resolution using the zoom technique, with only high-resolution DM particles ending up in the virial radius of the haloes at $z = 0$. Simulations are allowed to refine the initial mesh up to seven levels of refinement, which reach up to a $\Delta x = 1.1$ and 0.5 kpc physical length, respectively, for our low- and high-resolution initial conditions ($M_{\text{DM, res}} = 8.2 \times 10^7 M_{\odot}$ and $1.0 \times 10^7 M_{\odot}$). A cell is refined following a quasi-Lagrangian criterion: if more than eight dark matter particles lie in a cell, or if the baryon mass exceeds eight times the initial dark matter mass resolution.

Six haloes are simulated, five out of the $50 h^{-1} \text{ Mpc}$ simulation box at the highest resolution, and one (the most massive halo) is taken out of the $100 h^{-1} \text{ Mpc}$ simulation box at lower resolution. These six haloes are simulated with the same physics (gas cooling, star formation, metal cooling, SN feedback; see Section 2.2), and with one set without AGN feedback (GX simulations), and one set with AGN feedback as described in Section 2.3 (GXA simulations). Halo masses, DM particle mass resolution and minimum cell sizes are summarized in Table 1 together with some of the basic properties of the central galaxy at $z = 0$ [mass, colour, star formation rate (SFR)].

2.2 Physics of galaxy formation

Gas is allowed to radiate energy away and cool down to a minimum temperature of $T_0 = 10^4 \text{ K}$ due to atomic collisions in a gas of primordial composition, i.e. only H and He (Sutherland & Dopita 1993). We also account for the cooling enhancement due to the presence of metals released during supernovae (SNe) explosions from massive stars. Metals are passively advected with the gas, and their distribution depends on the history of the gas enrichment through SNe explosions. A fixed solar composition of heavy elements is

Table 1. Simulations performed with different sub-grid galactic models and different resolutions. (a) Name of the simulation. (b) Halo virial mass at $z = 0$. (c) Mass resolution of the high-resolution DM particles. (d) Stellar mass of the central galaxy at $z = 0$. (e) Minimum cell size. (f) Star formation efficiency. (g) Presence of AGN feedback (Y), or without AGN feedback (N). (h) $g - r$ relative colour magnitude of the central ETG accounting for dust extinction. (i) $g - r^*$ relative colour magnitude of the central ETG without dust extinction. (j) SFR of the central galaxy at $z = 0$.

(a) Name	(b) M_{vir} ($10^{13} M_{\odot}$)	(c) $M_{\text{res, DM}}$ ($10^7 M_{\odot}$)	(d) M_* ($10^{11} M_{\odot}$)	(e) Δx (kpc)	(f) ϵ_* (per cent)	(g) AGN	(h) $g - r$	(i) $g - r^*$	(j) SFR ($M_{\odot} \cdot \text{yr}^{-1}$)
G1	0.43	1.0	5.6	0.5	2	N	0.63	0.44	20
G1A	0.38	1.0	0.7	0.5	2	Y	0.71	0.68	0.2
G2	0.63	1.0	7.3	0.5	2	N	0.66	0.49	20
G2A	0.53	1.0	0.6	0.5	2	Y	0.73	0.73	<0.1
G3	1.0	1.0	13	0.5	2	N	0.62	0.46	50
G3A	1.0	1.0	2.3	0.5	2	Y	0.73	0.70	0.4
G4	1.7	1.0	20	0.5	2	N	0.67	0.48	50
G4A	1.5	1.0	3.2	0.5	2	Y	0.73	0.64	2
G5	2.4	1.0	27	0.5	2	N	0.59	0.42	100
G5A	2.3	1.0	5.4	0.5	2	Y	0.71	0.60	4
G6	8.0	8.2	81	1.1	2	N	0.66	0.45	250
G6A	8.0	8.2	13	1.1	2	Y	0.72	0.61	10

assumed for the computation of the gas cooling rates. Heating from a UV background is considered following Haardt & Madau (1996) during and after the redshift of reionization $z_{\text{reion}} \sim 6$.

Star formation in our model occurs in regions with gas number density $n > n_0 = 0.1 \text{ H cm}^{-3}$ using a random Poisson process to spawn star cluster particles, according to a Schmidt–Kennicutt law

$$\dot{\rho}_* = \epsilon_* \frac{\rho}{t_{\text{ff}}(\rho)}, \quad (1)$$

where ρ is the gas mass density, $\dot{\rho}_*$ the SFR mass density, ϵ_* the star formation efficiency and $t_{\text{ff}}(\rho)$ the gas free-fall time. In these simulations, we set the efficiency of star formation to a low value $\epsilon_* = 0.02$ that is in good agreement with observational surface density relationships of galaxies (Kennicutt 1998), and local giant molecular clouds (Krumholz & Tan 2007). Each star cluster particle has a mass resolution of $m_* = \rho_0 \Delta x^3$ (ρ_0 is the gas mass density threshold of star formation) where a random Poisson process is used to create a new star particle (Rasera & Teyssier 2006; Dubois & Teyssier 2008). The stellar mass resolution reaches $5.1 \times 10^5 M_{\odot}$ for our most resolved simulation with $\Delta x = 0.5 \text{ kpc}$. We ensure that no more than 90 per cent of the gas in a cell is depleted during the star formation process for numerical stability.

We account for the mass and energy release from Type II SNe assuming a Salpeter initial mass function (IMF). Using this IMF, 10 per cent of the massive stars above $8 M_{\odot}$ end their life into a Type II SN releasing 10^{51} erg per $10 M_{\odot}$. For each individual SN explosion, after 10 Myr, energy is released spherically in a kinetic mode transferring mass, momentum and energy with a mass loading parameter $f_w = 1$ that mimic a Sedov blast wave explosion (see Dubois & Teyssier 2008, for further details). We assume that Type II SNe release all their mass into the gas (no stellar remnant forms) with a $y = 0.1$ stellar yield, which is the fraction of primordial gas transformed into heavy elements and released back into the gas. With this prescription, we do not take into account the energy and mass release from stellar winds (AGB stars), nor from long-lived Type Ia SNe.

The gas follows an adiabatic equation of state with an adiabatic index $\gamma_{\text{adiab}} = 5/3$. In order to take into account the thermal impact

of the heating of the gas by SNe, we modify the temperature at high gas density $\rho > \rho_0$ with a polytropic equation of state

$$T = T_0 \left(\frac{\rho}{\rho_0} \right)^{p-1}, \quad (2)$$

where p is the polytropic index of the gas. The adopted value of $p = 4/3$ is comparable to the value obtained in Springel & Hernquist (2003) considering the multiphase structure of the ISM with stellar heating. We point out that this value of $p = 4/3$ does not rigorously ensure that gas fragmentation is avoided due to numerical instabilities (Truelove et al. 1997), as the Jeans length is proportional to the gas density

$$\lambda_J = 10.7 \left(\frac{\rho}{0.1 \text{ H cm}^{-3}} \right)^{-1/3} \text{ kpc}. \quad (3)$$

This last formula shows that at very high gas densities, the Jeans length can be smaller than our minimum resolution and would provide spurious fragmentation of the gas. However, the gas cannot indefinitely condense because of the finite force resolution sampling and the star formation process that removes gas in high-density regions.

2.3 AGN feedback

Our modelling of AGN feedback closely follows the implementation detailed in Dubois et al. (2012). We recall here the main aspects of this modelling, and refer to Dubois et al. (2010, 2012) for the technical issues. BH particles are modelled with the sink particles technique from Bate, Bonnell & Price (1995), and particularly Krumholz, McKee & Klein (2004) for mesh codes. The BHs are created in the centres of galaxies, with a sufficiently large exclusion radius (100 kpc) to prevent formation of multiple massive BHs per galaxy. The initial BH seed mass is chosen to be $10^5 M_{\odot}$. BHs can merge when they are sufficiently close to one another ($< 4 \Delta x$), determined using a Friend-Of-Friends algorithm on sink particles performed on-the-fly.

BHs can grow by accretion at a Bondi–Hoyle–Lyttleton rate (Bondi 1952)

$$\dot{M}_{\text{BH}} = \frac{4\pi\alpha G^2 M_{\text{BH}}^2 \bar{\rho}}{(\bar{c}_s^2 + \bar{u}^2)^{3/2}}, \quad (4)$$

where G is the gravitational constant, $\bar{\rho}$ the average gas mass density, \bar{c}_s the average sound speed, \bar{u} the average gas velocity relative to the BH and α a dimensionless boost factor with $\alpha = (\rho/\rho_0)^2$ when $\rho > \rho_0$ and $\alpha = 1$ in order to account for our inability to capture the cold and high-density regions of the gas at these kpc resolutions that would substantially increase the accretion rate if these regions were resolved as suggested in Booth & Schaye (2009).

The accretion rate on to BHs is limited by its Eddington rate

$$\dot{M}_{\text{Edd}} = \frac{4\pi G M_{\text{BH}} m_p}{\epsilon_r \sigma_T c}, \quad (5)$$

where σ_T is the Thompson cross-section, c is the speed of light, m_p is the proton mass and ϵ_r is the radiative efficiency, assumed to be equal to 0.1 for the Shakura & Sunyaev (1973) accretion on to a Schwarzschild BH.

A drag force is applied to the BH particles in order to replicate the action of dynamical friction of the gas on massive BHs that happens on unresolved parsec scales. The dynamical friction force is defined as

$$F_{\text{DF}} = f_{\text{gas}} 4\pi\alpha\bar{\rho} \left(\frac{GM_{\text{BH}}}{\bar{c}_s} \right)^2, \quad (6)$$

where f_{gas} is a fudge factor whose value is between 0 and 2 and is a function of the Mach number $\mathcal{M} = \bar{u}/\bar{c}_s < 1$ (Ostriker 1999; Chapon, Mayer & Teyssier 2013), and where α is the boost factor already introduced in equation (4). This extra force term for BH dynamics has been successfully introduced in high-redshift simulations with ~ 10 pc resolution to maintain BHs close to the centre of the galaxy (Dubois et al. 2013).

In this paper, we assume that AGN feedback proceeds uniquely in the jet mode powering large bipolar outflows. The total energy released by the AGN is

$$\dot{E}_{\text{AGN}} = \epsilon_f L_r = \epsilon_f \epsilon_r \dot{M}_{\text{BH}} c^2, \quad (7)$$

where $\epsilon_f = 1$ is a free parameter chosen to reproduce the $M_{\text{BH}}-M_b$, $M_{\text{BH}}-\sigma_b$ and BH mass density in our local Universe (see Dubois et al. 2012). For this jet mode of AGN feedback, mass, momentum and kinetic energy are continuously released in the surrounding gas along a jet axis defined by the local angular momentum of the gas, and such that the jet velocity is 10^4 km s^{-1} , or equivalently the mass loading factor of the jet is $\eta = 100$.

3 RESULTS

3.1 Changing the baryon content and the morphologies of massive galaxies

The basic picture of the formation of massive haloes is that they form at high redshift by cold filamentary infall driving high levels of star formation, and at low redshift by a fainter diffuse (and hot) accretion, as illustrated for the halo G5A in Fig. 1 (Rees & Ostriker 1977; White & Frenk 1991; Birnboim & Dekel 2003; Kereš et al. 2005; Ocvirk et al. 2008; Dekel et al. 2009a; van de Voort et al. 2011). For groups of galaxies, satellites represent a non-negligible fraction of the total stellar mass in the halo with the large number of satellites orbiting inside the virial radius of the halo. Note that some of these satellites have no dense star-forming gas

component. This gas has been stripped away by the ram pressure of the hot diffuse gas as can be seen for some satellites with tails of gas.

Massive haloes usually suffer from over-cooling of their gas content in absence of any strong feedback prescription. Vanilla hydrodynamical simulations (i.e. without any strong feedback) produce large amount of stars in massive central galaxies as shown in Fig. 2. The measured stellar mass M_s is given by the total stellar mass of the central galaxy as detected by the AdaptaHOP algorithm (Aubert, Pichon & Colombi 2004; Tweed et al. 2009) performed on stars, and, thus, captures the stellar content in the core of the halo together with its related intra-cluster light, and removes all satellites (considered as ‘sub-galaxies’ of the central most massive galaxy). The halo mass M_h is the total mass of gas, stars, DM (and BHs if any) enclosed within the virial radius provided by the halo finder algorithm (using AdaptaHOP on DM particles). In the absence of AGN feedback, stars are converted in the central galaxy with a $f_{\text{conv}} = 0.7$ global efficiency, where $f_{\text{conv}} = M_s/f_b M_h$ and $f_b = \Omega_b/\Omega_m = 0.165$, while observations (e.g. from Moster et al. 2010) suggest that the value for groups of galaxies is 0.1 (for a halo mass of $M_h \simeq 10^{13} M_\odot$) and decreases with increasing halo mass. AGN feedback manages to reduce the stellar mass of the central massive galaxies at $z = 0$ by a factor of 7 compared to the no AGN feedback case, but these galaxies still remain too massive, in particular even for those belonging to the most massive haloes.

Note that if, as suggested by recent observations using lensing (or dynamics) and photometry (Grillo et al. 2008; Auger et al. 2010; Grillo & Gobat 2010; Treu et al. 2010; Spiniello et al. 2011; Thomas et al. 2011; Sonnenfeld et al. 2012; Cappellari et al. 2013) or spectroscopy (Conroy & van Dokkum 2012; Spiniello et al. 2012), the IMF is considered to be more bottom-heavy for the most massive galaxies, then the observational relation of M_s versus M_h should be pushed towards higher values of M_s . Assuming a Salpeter (1955) IMF instead of a Kroupa (2001) (or Chabrier 2003) IMF, the ratio M_s/M_h increases by +0.3 dex, which puts our values of the central stellar mass for the four most massive galaxies (with AGN feedback) in better agreement with observations, but in less better agreement for the two least massive galaxies (G1A and G2A). There is probably a smooth transition from a Kroupa to a Salpeter IMF for galaxies with velocity dispersion around $100\text{--}200 \text{ km s}^{-1}$ (Cappellari et al. 2013), values which correspond to the typical ones of the galaxies at $z = 0$ when simulated with AGN feedback (see Section 3.3).

Fig. 3 shows the evolution of the stellar conversion efficiency f_{conv} averaged over the six central galaxies as a function of redshift. In the absence of AGN feedback, f_{conv} is continuously increasing with decreasing redshift. Large amounts of gas are piling up in the central galaxy due to over-cooling, but, as it takes several free-fall times ($t_{\text{ff}}/\epsilon_* = 50t_{\text{ff}} \simeq 1 \text{ Gyr}$ for a typical gas number density of $n = 10 \text{ cm}^{-3}$ in star-forming regions; see Fig. 1) to convert the cold gas content into stars, the value of f_{conv} is lower at high redshift. The same trend for the evolution of f_{conv} is observed at high redshift above $z \sim 2$ for the simulations with AGN feedback. However, during the early phase of galaxy formation, the presence of AGN feedback allows for a rapid quenching of the star formation with a reduced value of f_{conv} by a factor of 2 at $z = 3\text{--}4$ compared to galaxies simulated without AGN. From $z \sim 2$ to $z = 0$, the value of f_{conv} slowly decreases by a factor of 2. While haloes continue to grow by diffuse accretion and mergers, the gas is efficiently prevented to cool further down by AGN feedback, and the central galaxy stops actively forming stars (see the values of the SFR obtained at $z = 0$ in Table 1).

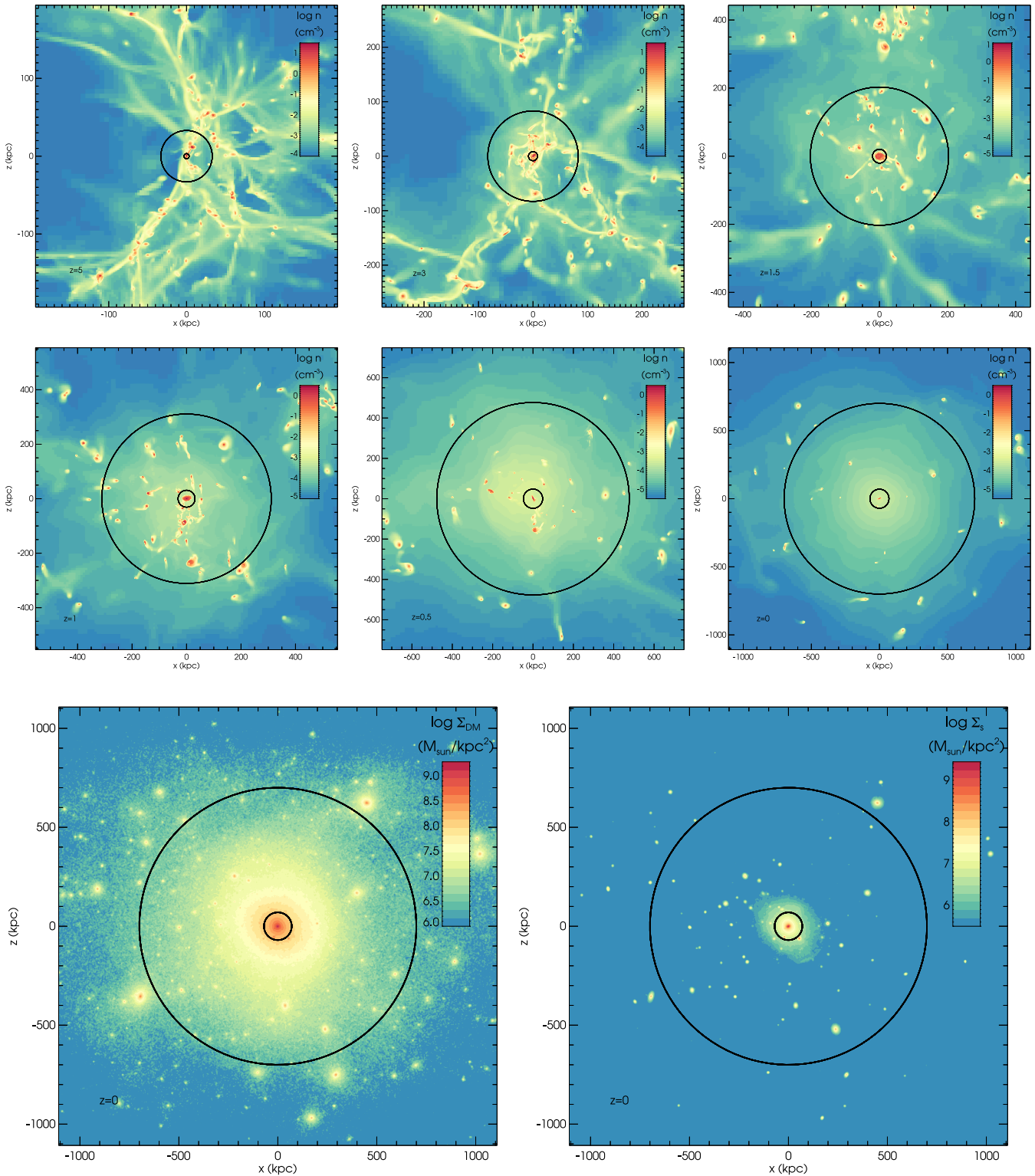


Figure 1. Top and middle rows: images of the projected gas number density at $z = 5$ (top left), $z = 3$ (top centre), $z = 1.5$ (top right), $z = 1$ (middle left), $z = 0.5$ (middle centre) and $z = 0$ (middle right) around the most massive galaxy of the G5A simulation; and (bottom) images of the projected DM surface density (left), and stellar surface density (right) at $z = 0$. The large circles correspond to the virial radius of the host halo and the small circles to 10 per cent of the virial radius. The image sizes are in physical length. The gas distribution around the central galaxy shows a complex filamentary network at high redshift, and a smooth spherical distribution of gas with a large number of satellites at intermediate and low redshift.

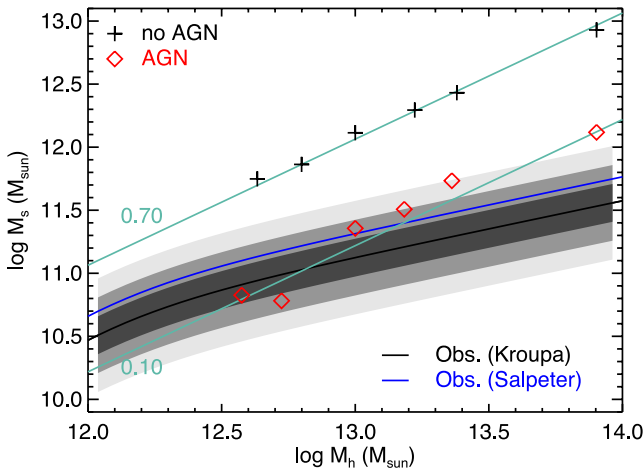


Figure 2. Stellar mass of central massive galaxies as a function of their halo mass at $z = 0$ for the simulations without AGN (black), and for the simulations with AGN feedback (red). The solid curves are the observational fit from Moster et al. (2010) either assuming a Kroupa (black) or a Salpeter (blue) IMF, with the 1σ , 2σ and 3σ standard deviation (grey shaded areas). Cyan solid lines indicate the amount of stars formed at a constant efficiency $f_{\text{conv}} = M_s/f_b M_h$. The presence of AGN feedback reduces the total amount of stars in the central massive galaxy by a factor of 7.

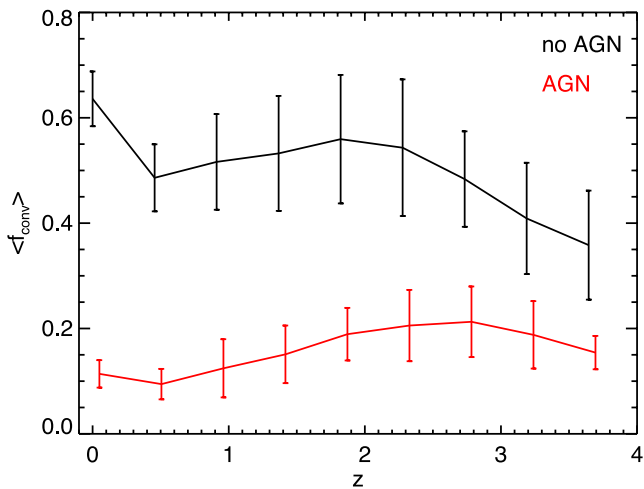


Figure 3. Average conversion efficiency of the central galaxies $f_{\text{conv}} = M_s/f_b M_h$ as a function of redshift for the simulations including AGN feedback (red) or without AGN feedback (black) with the standard deviation (error bars). The values are averaged over the main progenitor of the central galaxy for the six haloes. The conversion efficiency of stars in the central galaxy is strongly reduced by the presence of AGN feedback and the reduction takes place already at high redshift (a factor of 2 reduction at $z = 4$).

The presence of AGN shuts down the star formation in the central galaxies and it starts already at high redshift. The specific Star Formation Rate (sSFR) (see Fig. 4) is continuously decreasing with time due to the starvation of the reservoir of cold gas by the cosmological growth of structures, and the activity of the central AGN that exacerbates the depletion of gas in massive galaxies. At high redshift, central BHs accrete gas close to the Eddington ratio while at low redshift they experience long periods of time without accreting gas and with intense burst of AGN activity driven by mergers and cooling flows (see Fig. 5). Even though there is a lot less gas available in galaxies at low redshift, and that the AGN activity is

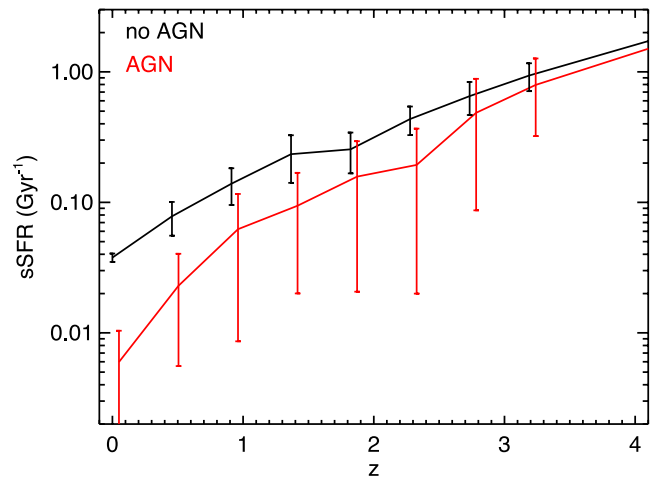


Figure 4. Average sSFR as a function of redshift for the central galaxy of the six simulated haloes with (red) or without (black) AGN feedback, with the standard deviation (error bars). The presence of AGN feedback diminishes the sSFR by a factor of ~ 5 at $z = 0$.

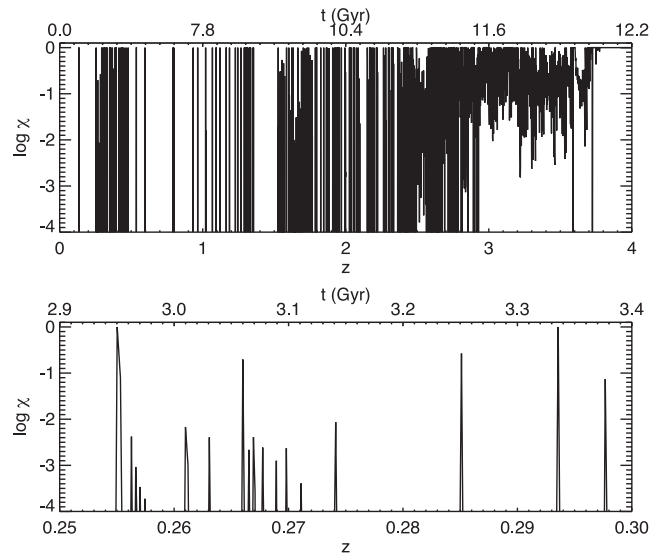


Figure 5. Instantaneous accretion rate over Eddington rate χ as a function of redshift (or lookback time) for the central BH of the G6A galaxy over the redshift range $z = 0-4$ (top panel), and zoomed over the redshift range $z = 0.25-0.3$. The Eddington ratio is maximum at high redshift with values close to ~ 1 , and with brief episodes of accretion on to BHs (i.e. AGN activity) at low redshift that help to regulate the cold baryon content in the central massive galaxy.

overall greatly diminished, bursts of AGN activity are necessary to self-regulate the cold baryon content in galaxies at low redshift (Dubois et al. 2011).

By simulating the stellar light emission (using the SDSS u , g and r filter bands) of the central galaxies, we observe that, because of AGN feedback, they become less luminous, more red and with rounder shapes (see Fig. 6). In the absence of AGN feedback, the central galaxies exhibit a massive blue disc component (with spiral arms for some of them) in their centres, that is confirmed by the measured colours, around $g - r = 0.45$ without dust extinction. For instance some simulations without AGN feedback show a massive blue component, which is associated with a disc with spiral arms. For these over-massive objects, there is a strong dust lane component

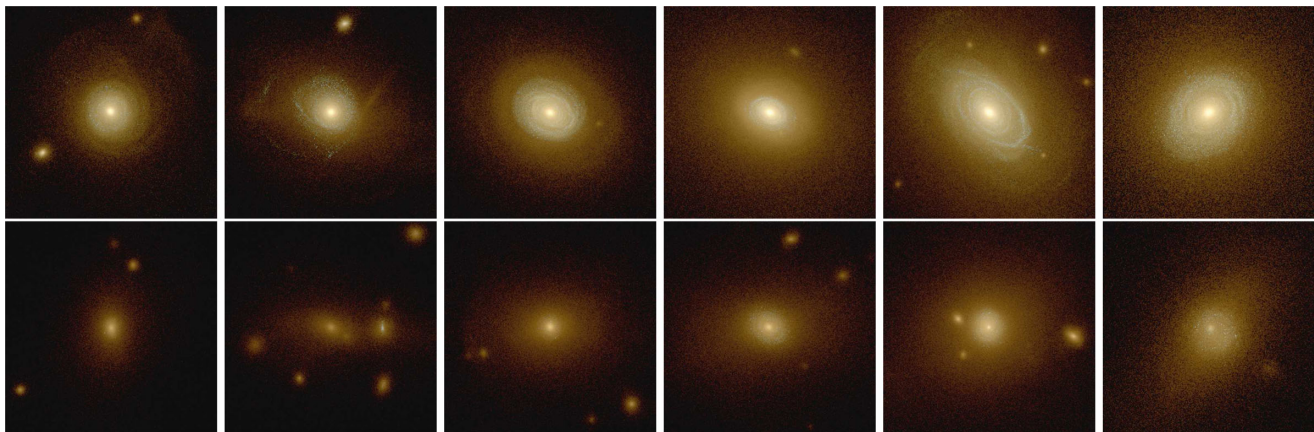


Figure 6. Stellar emission of the central galaxies from G1 to G6 (left to right) without (top) or with AGN feedback (bottom) at $z = 0$, as they would be observed in $u-g-r$ filter bands. Extinction by dust is not taken into account in these images. Arbitrary units are used for stellar emission but with similar minima and maxima for all the first fifth columns, and with decreased intensities by 0.5 dex for the last column to avoid image saturation. The size of each panel is 140 kpc. Galaxies without AGN feedback exhibit a massive blue disc component with a halo of stars extending to large distance. AGN feedback reduces the total amount of emitted light, and galaxies appear more early type with a weak disc component for some of them.

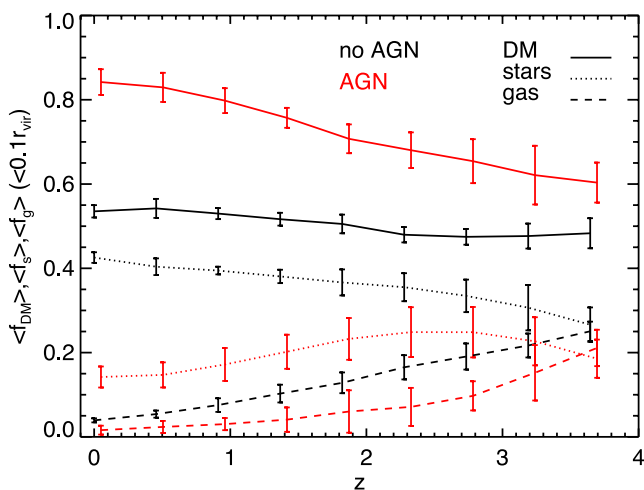


Figure 7. Average fraction of DM (solid), stellar (dotted) and gas (dashed) mass within $0.1r_{\text{vir}}$ as a function of redshift for the six haloes with (red) or without (black) AGN feedback. The error bars are the standard deviation. The fraction of DM mass is increased, and the fractions of gas and stellar mass are decreased by the effect of AGN feedback.

(not represented in the images of Fig. 6), which reddens them by $\Delta(g-r)_{\text{dust}} = 0.2$ (see Table 1). In contrast, simulated galaxies with AGN feedback have colours between $0.60 < g-r < 0.73$ (no dust extinction), and for some of them a contribution is adopted for dust extinction of $\Delta(g-r)_{\text{dust}} = 0.1$ (closer to zero for some others). We get better consistency of galaxy colours with observations when AGN feedback is considered (Bernardi et al. 2005).

We measure the average mass fractions of DM, stars and gas within the $0.1r_{\text{vir}}$ of the halo as a function of redshift for the simulations with or without AGN feedback (Fig. 7). We find that the fraction of DM mass is more important in the core of haloes when AGN feedback is present, going from $\langle f_{\text{DM}} \rangle = 0.53$ without AGN up to $\langle f_{\text{DM}} \rangle = 0.83$ with AGN at $z = 0$. The DM fraction is constant over time in the absence of AGN feedback, but increases with time for the AGN case. Note that the DM fraction is already higher in the AGN case at high redshift compared to the no AGN case, but this difference is enhanced at low redshift. Without AGN feedback

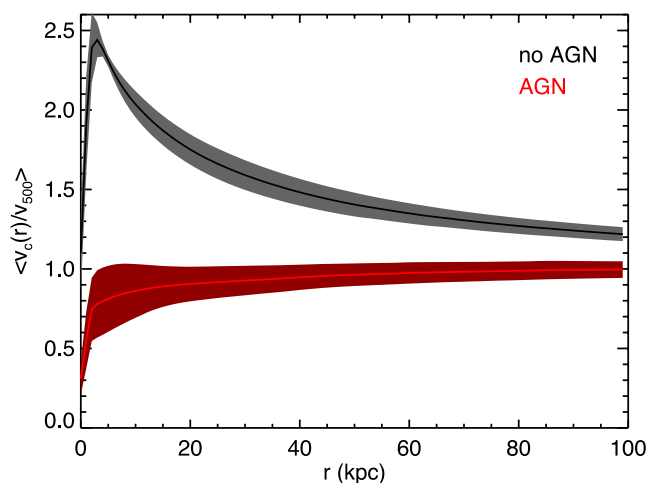


Figure 8. Circular velocities averaged over the six haloes with (red) or without (black) AGN feedback as a function of radius at $z = 0$. Velocities are renormalized by the circular velocities at r_{500} . Shaded areas correspond to the standard deviation. Simulations without AGN feedback exhibit a central peak in the circular velocity that is characteristic of too large mass concentration in the centre of the galaxy, while simulations with AGN feedback show flat velocity curves with a value close to the circular velocity at r_{500} .

the fraction of stars is increasing with time and the gas fraction is decreasing, while the baryonic fraction is constant (DM fraction is constant). Thus, galaxies are gas-rich (wet) at high redshift, and gas-poor at low redshift because they consume the gas efficiently in the star formation process. Both the stellar and the gas mass fractions are reduced due to the presence of AGN feedback, from $\langle f_s \rangle = 0.42$ down to $\langle f_s \rangle = 0.15$, and from $\langle f_g \rangle = 0.04$ down to $\langle f_g \rangle = 0.016$ at $z = 0$. The difference in stellar and gas mass fractions is also seen at higher redshift, but in smaller proportions than at low redshift. Finally, AGN feedback already impacts the mass content in galaxies early on (at $z \sim 4$), but its effect is largest at $z = 0$.

Thanks to an exquisite resolution, we are able to go beyond the global properties listed above and investigate the internal dynamical structure of galaxies. The morphology of galaxies is also transformed by the effect of AGN feedback as shown in Fig. 8.

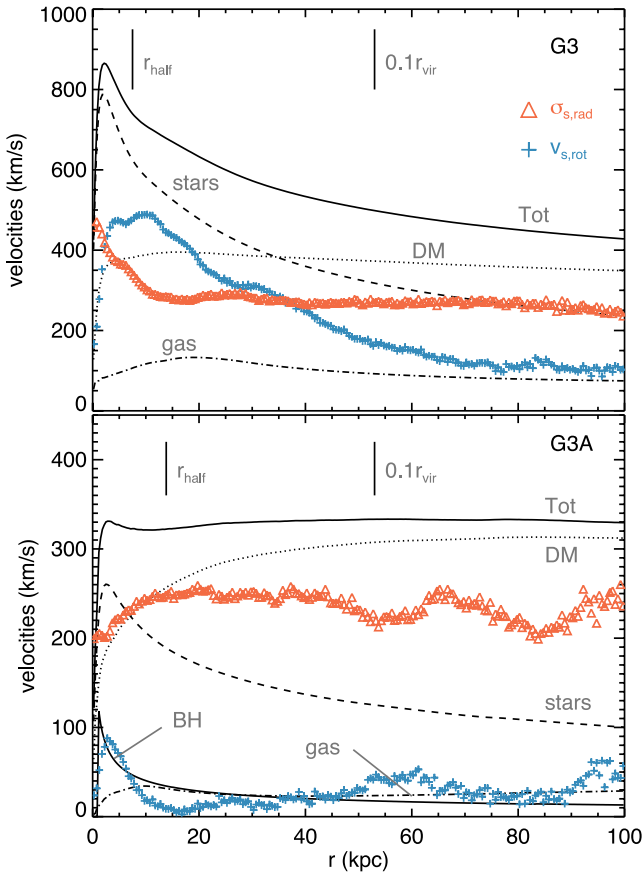


Figure 9. Illustration of the morphological transformation of the central massive galaxy of the halo of G3 at $z = 0$ due to AGN feedback. Both panels show the circular velocities as a function of radius (black) of all components (solid), stars (dashed), DM (dotted), gas (dot-dashed) and BHs (triple dot-dashed) without AGN feedback (top panel), or including AGN feedback (bottom panel). The measured rotational velocities for stars $v_{s,rot}$ (blue plus) and radial velocity dispersions $\sigma_{s,rad}$ (orange triangle) are also indicated. The 3D stellar half-mass radius r_{half} and 10 per cent of the virial radius $0.1r_{vir}$ are indicated as vertical bars. The circular velocity is decreased by a factor of 2 due to AGN feedback. The circular velocity is dominated by the stellar component up to large distance (30 kpc) in the AGN case, while it dominates only in the very central region (7 kpc) in the AGN case, and the DM is the principal contributor outside these characteristic radius. The galaxy is transformed from a rotating disc (no AGN case) into a velocity dispersion-dominated ellipsoid (AGN case).

Circular velocities $v_c = \sqrt{GM_{tot}(<r)/r}$ exhibit a peak close to the centre of the galaxy, below 5 kpc, when AGN feedback is not included. This peak is produced by the large concentration of material in the central region of galaxies, where the total matter distribution is largely dominated by stars (see Fig. 9), and is a characteristic feature of the overcooling problem of baryons (e.g. Few et al. 2012; Scannapieco et al. 2012). In the opposite case, for the simulations including AGN feedback, the peak in the circular velocity profiles disappears and profiles become flat (isothermal) up to very large distances away from the centre, with values close to the circular velocity measured far away from the centre (at r_{500}). With the presence of AGN feedback, the maximum of the circular velocity curves decreases, the contribution from stars to circular velocity is strongly attenuated, and replaced by its DM component (Fig. 9). Note that the contribution from gas to the circular velocity curves at $z = 0$ is negligible with or without AGN feedback, which suggests that

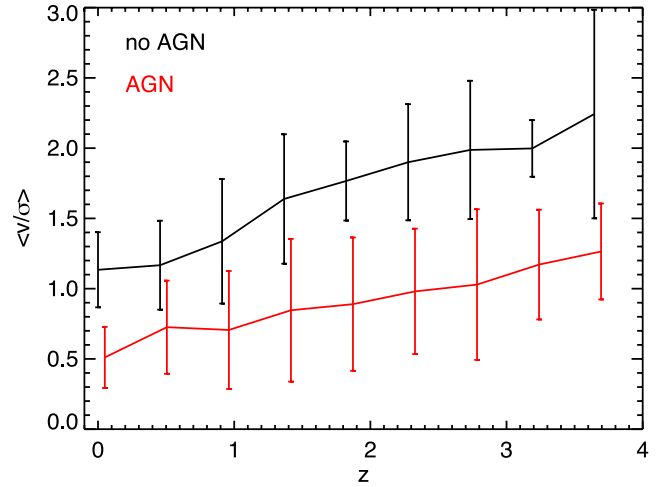


Figure 10. Average v/σ ratio as a function of redshift for the central galaxy of the six simulated haloes with (red) or without (black) AGN feedback, with the standard deviation (error bars). The galaxies simulated without AGN feedback are fast rotators at any redshift, while galaxies simulated with AGN feedback are slow rotators.

these massive galaxies are relatively gas-poor independently of the presence of AGN. We notice that the ratio of radial velocity dispersion over the circular velocity is roughly constant and close to a factor of $\sqrt{2}$; therefore, it gives further evidence for an isothermal profile. It assumes that orbits are isotropic, i.e. the velocity tensor is close to isotropic. Further investigations along this line are left for future work.

AGN have also important consequences for the total amount of rotation and velocity dispersion in these massive galaxies. Without AGN feedback, the stellar component of the massive galaxies at $z = 0$ is supported by the rotation of stars, with a comparable but lower contribution from dispersion, particularly within the half-mass radius of the galaxy. Such galaxies would be classified as fast rotators as the v/σ ratio for stars approaches one (even though their masses and colours are unrealistic). At a close distance from the centre, the velocity support is dominated by the dispersion (compact bulge of stars), and also far away, in the intra cluster light. The picture is changed when AGN feedback is present: velocity dispersion dominates at any distance from the centre at $z = 0$. The disc component has considerably shrank and, now, is barely detectable below 5 kph at $z = 0$ (Fig. 9).

Fig. 10 shows the average v/σ ratio, where v is the mass-weighted rotational velocity of stars and σ is the mass-weighted velocity dispersion of stars measured within r_{eff} , where r_{eff} is the effective radius at which half of the projected stellar mass is enclosed. Both quantities are integrated quantities of the projected distribution of stars, and the v/σ ratios showed in Fig. 10 are averaged over the six galaxies (with or without AGN feedback). Without AGN feedback, the galaxies have large values of v/σ above 1, i.e. are dominated by the rotation of stars at all redshifts. Due to the increased proportion of accreted material (see the next section), the v/σ ratio decreases with time and tends towards 1 at $z = 0$. Thus the massive galaxies at $z = 0$ simulated without AGN feedback are disc-like galaxies. The transformation of rotationally supported discs into dispersion-dominated ellipsoids by the presence of AGN feedback is observed for all our simulated central galaxies at low redshift ($z < 1$). The same evolution is found for galaxies simulated with AGN feedback as without AGN feedback: the ratio of v/σ also decreases with time, but AGN transforms the galaxies into slow rotators ($v/\sigma < 1$) where

galaxies become essentially supported by the velocity dispersion of the stars, with a value slightly above 1 at $z = 4$ down to a value of 0.5 at $z = 0$. The importance of rotation over dispersion is already reduced by a factor of 2 at high redshift ($z = 3-4$).

We interpret this morphological change as the signature that massive galaxies are transformed from systems dominated by in situ star formation (without AGN feedback) into systems dominated by accretion of satellites (with the presence of AGN). We will now clearly demonstrate this mechanism in the following section.

3.2 From in situ to accretion-dominated systems

The fraction of stars locked into satellites $M_{s, \text{sat}}/M_{s, \text{tot}}$, where $M_{s, \text{sat}}$ is the mass of stars in satellites within r_{vir} , and $M_{s, \text{tot}}$ is the total mass of stars within r_{vir} , is increasing with time and reaches values of 20–30 per cent at $z \simeq 0$ without AGN and 40–50 per cent with AGN (see Fig. 11). When AGN feedback is active, it efficiently reduces the total stellar mass in the central galaxy (Fig. 3) by blowing gas away and preventing gas accretion. The increased fraction of mass locked into galaxy satellites due to AGN is a clear indicator that the mass build-up of central galaxies should have a decreased proportion of stellar mass formed in the main progenitor. The shapes of the curves are similar for AGN and no AGN cases. This is due to the fact that the presence of AGN does not affect the merger history of haloes that are dominated by the DM component.

To demonstrate the effect of AGN feedback on the stellar mass build-up, we define the in situ formed stars as the stars formed within the main progenitor of the galaxy (within 10 per cent of the virial radius of the host halo), and the *accreted* stars are defined to be the stars formed outside of the main progenitor of the galaxy and acquired through capture of satellites or by diffuse accretion. Fig. 12 shows the amount of stellar mass in the central massive galaxy formed in situ and the amount of stars that are accreted, for the different simulations, depending on the presence of AGN feedback. Galaxies are dominated by the in situ growth of the stellar mass at high redshift due to the large fraction of baryons available in the form of cold star-forming gas (Daddi et al. 2010; Tacconi et al. 2010; Dubois et al. 2012). As a consequence, the sSFRs (SFR

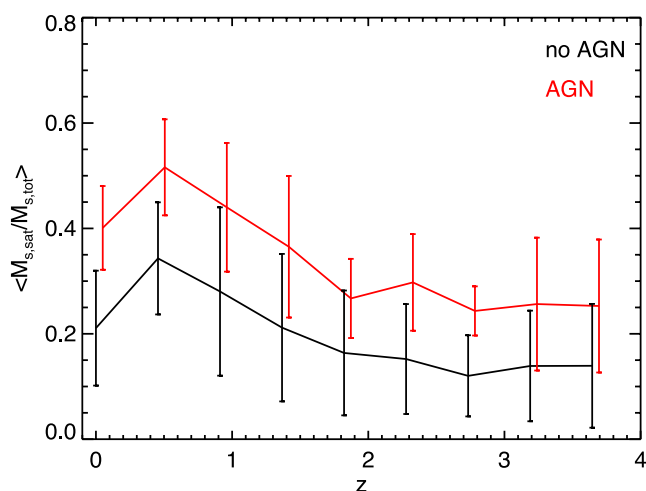


Figure 11. Average fraction of the total stellar mass in the halo locked into satellite galaxies without AGN feedback (black) and with AGN feedback (red). The values are averaged over the six simulated haloes, and the error bars correspond to the standard dispersion. With the presence of AGN feedback, the fraction of stars locked into the galaxy satellites is increased with almost half of it in the satellites at $z = 0$.

per galaxy stellar mass) are maintained at high values, even when AGN feedback is included (Kimm et al. 2012). Conselice et al. (2013) have shown that observed massive galaxies $M_s > 10^{11} M_\odot$ acquire the majority of their stars 61 ± 21 per cent through the in situ star formation between redshift $1.5 < z < 3$ which is consistent with our findings. As time goes on, the gas reservoir is consumed in the star formation process and ejected through the galactic winds produced by AGN feedback, and the sSFRs decline. The result is that mergers have an increasing contribution to the mass build-up of these massive galaxies (De Lucia & Blaizot 2007), and the fraction of in situ formed stars declines with time (decreasing redshift) as seen for all the six simulated haloes independently of the presence of feedback.

The difference between the two simulation types (with or without AGN) is that, for the ‘vanilla’ model (no AGN), the central galaxy mass is dominated by the in situ star formation (stars are formed locally) at $z = 0$ with $f_{\text{in situ}} \simeq 55$ per cent of the total stellar mass on average, while, for the AGN feedback runs, the stellar mass is dominated by the accretion of satellites at $z = 0$ with $f_{\text{in situ}} = 40$ per cent on average, as seen in Fig. 13. It is important to stress that *both* the mass of in situ formed stars and the mass of accreted stars at $z = 0$ are decreased because of the presence of AGN feedback (Fig. 12), *but* AGN feedback quenches the star formation more efficiently in the central galaxy than it does in the galaxy satellites. Note that, as suggested by Fig. 3, the total mass of stars in the central galaxy is already affected by the presence of AGN feedback early on ($z = 3-4$), and that the fraction of in situ formed stars is decreased early on when the activity of AGN is the strongest (Dubois et al. 2012).

As seen in the previous section (see Figs 9 and 10), the galaxies are transformed from rotationally supported (discs) into dispersion dominated (ellipticals) systems. We will show that this is a direct consequence of the transformation of galaxies being build-up by in situ star formation (without AGN) into accretion-dominated systems (with AGN), and that the transformation has important implications for the dynamical properties of these objects. As an illustration, Fig. 14 shows the stellar density profiles of the central galaxy G4 and the central galaxy G4A at $z = 0$, decomposed into in situ and accretion components. The in situ component dominates the total stellar density profile in the core of the galaxy, whereas the accreted material dominates in the outskirts. This is a natural outcome of the in situ stars forming in the depth of gravitational potentials, and the satellites being tidally stripped while falling into haloes on elliptical orbits, thus depositing accreted stars far away from the centre (Naab et al. 2009; Peirani et al. 2010; Hilz et al. 2012).

AGN feedback changes the radius at which the transition between an in situ dominated density towards an accretion-dominated density occurs. As the proportion of accreted material is increased due to the efficient quenching of the in situ star formation by AGN feedback, the radius at which accreted material dominates is pushed towards the interior part of the halo (e.g. from 24 to 14 kpc for the G4X halo at $z = 0$; see Fig. 14). Note that the stellar density profiles are steeper than isothermal in both cases with a slightly flatter profile within 10 kpc for the AGN case than for the no AGN case. The effective radius (or half-mass radius for 3D profiles) associated with the accreted material is larger than those of the in situ component. It results that galaxies get puffed up due to the presence of AGN feedback because it enhances the fraction of accreted material by quenching the in situ star formation. The size increase is orchestrated by the subsequent merger events and the scaling of size with mass depends also on the initial structural

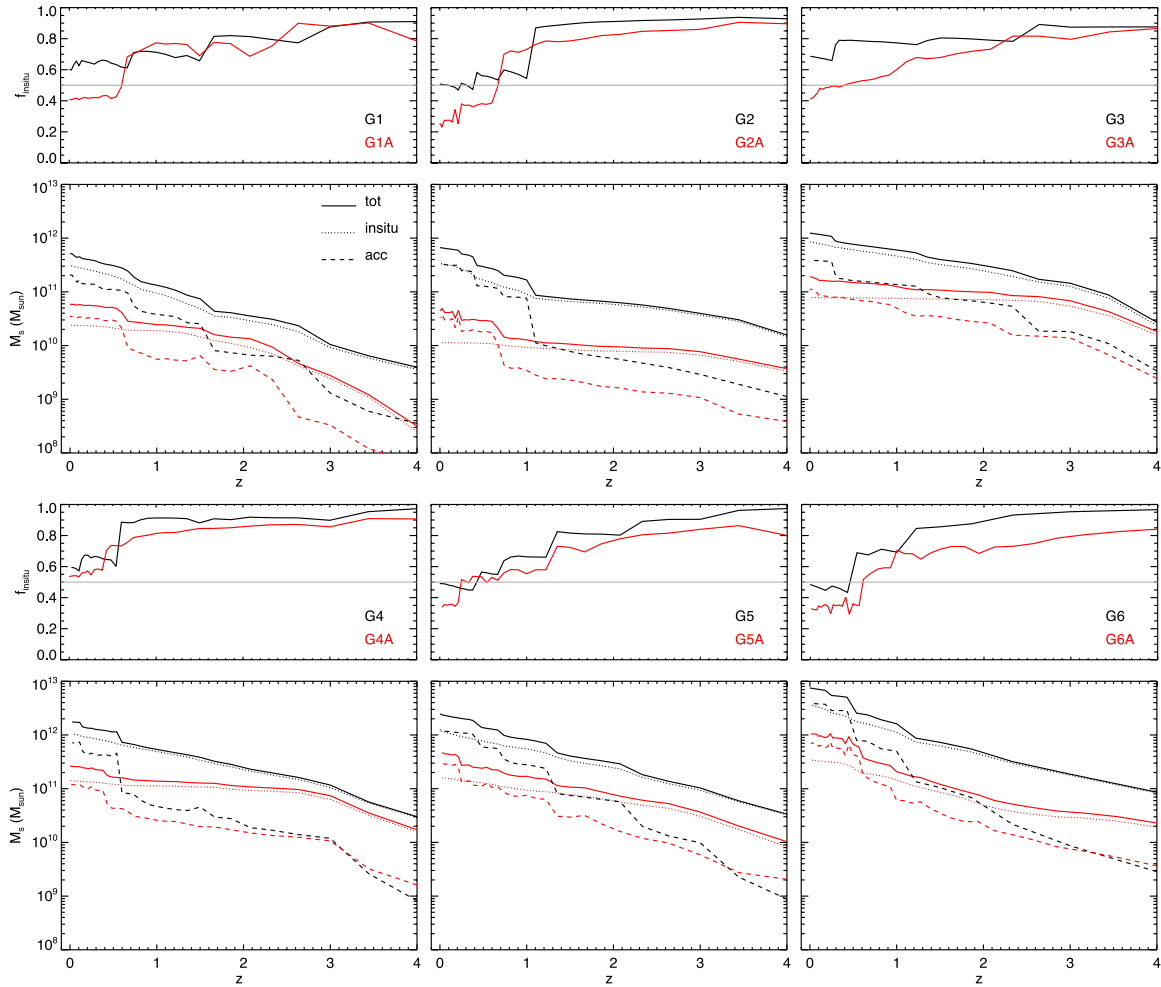


Figure 12. Top: fraction of in situ formed stars and, bottom: total stellar mass (solid lines), mass of in situ formed stars (dotted lines) and of accreted stars (dashed lines) as a function of redshift for G1 (top left), G2 (top middle), G3 (top right), G4 (bottom left), G5 (bottom middle) and G6 (bottom right). The results for simulations without AGN feedback are in black (GX) and with AGN feedback in red (GXA). The grey horizontal lines indicate the 50 per cent level of in situ versus accreted stellar mass.

properties of the progenitor galaxies at higher redshift (see Laporte et al. 2012; Oser et al. 2012).

Fig. 15 shows the evolution in redshift of the effective radius, and the in situ and accreted effective radii for all haloes with or without AGN feedback. All simulations show a larger value of their effective radii in the cases with AGN feedback, which is a direct consequence of the mechanism described above: as accretion has a more important role, galaxy sizes are increased. This mechanism is also confirmed by the fact that high-redshift effective radii are closer to their in situ effective radii, while low-redshift effective radii are closer to the accreted effective radii (respectively when in situ, or accreted mass dominates; see Fig. 12). The average logarithmic slope of the evolution of the effective radius with redshift $d \log r_{\text{eff}}/dz$ measured between redshift 0 and 2 is equal to -0.23 in the case without AGN feedback, and to -0.39 in the case with AGN feedback. Thus, the effective radius of galaxies simulated with AGN feedback evolves faster with time than galaxies without AGN. This is a direct consequence of the galaxies having an increased fraction of accreted material in their mass assembly in the former case.

The effective radius of the accreted material is increased for all galaxies with the presence of AGN feedback between $0 \leq z \lesssim 1$ (dashed lines in Fig. 15), where the sharp transition from in

situ to accreted dominated galaxies occurs (Fig. 13). The explanation is that tidal stripping becomes more efficient at removing stars from satellites. The characteristic radius above which tidal stripping can remove material from a satellite is (King 1962) $r_{\text{ts}} = D(0.5M_{\text{sat}}/M_s)^{0.5}$ where D is the distance between the central galaxy and the satellite. The distance at which satellites start losing stars is when $r_{\text{ts}} < r_{\text{eff}}$, or $D < r_{\text{eff}}(2M_s/M_{\text{sat}})^{0.5}$. Thus, if galaxies are less compact (i.e. they have larger effective radii), satellites will be more subject to tidal stripping early on, and will lose their stars at larger distances. This is compatible with the fact that galaxies are less compact with AGN feedback as observed from our simulations.

The behaviour of the effective radius of the in situ component together with the effect of AGN feedback shows more variations (dotted lines in Fig. 15). Some simulated galaxies show an increase of their in situ effective radius, while some others have a more compact in situ stellar content. We identify two effects that can act in opposite directions. As galaxies build from inside out in the classical picture of gas accretion, galactic discs of gas tend to be smaller due to strong AGN feedback as the accretion is quenched on to galaxies, an effect which can potentially decrease the size of the in situ component. On the other hand, strong bursts of feedback have been identified as creating strong variations in the gravitational potential

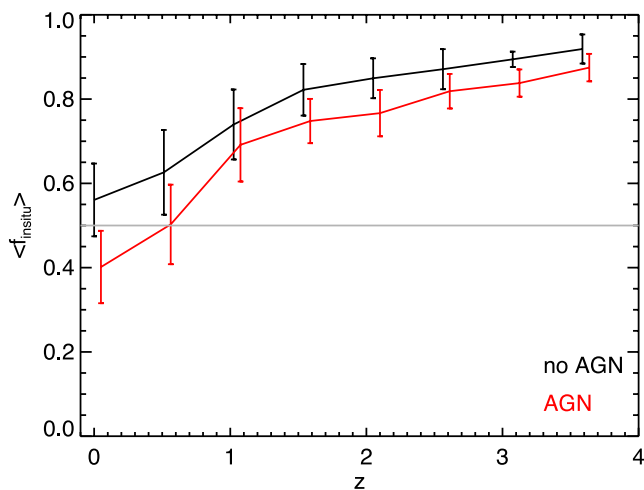


Figure 13. Average fraction of in situ formed stars as a function of redshift without AGN feedback (black) and with AGN feedback (red). The grey horizontal lines indicate the 50 per cent level of in situ versus accreted stellar mass. The error bars indicate the standard deviation to the average value. The in situ fraction of stars decline with time, and the presence of AGN feedback reduces this fraction further down to turn galaxies into accretion-dominated systems at $z = 0$.

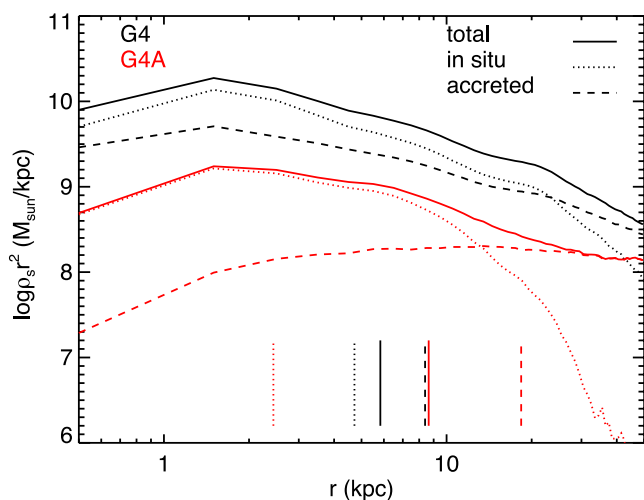


Figure 14. Total stellar density profiles multiplied by r^2 (solid lines) as a function of radius at $z = 0$ for the central galaxy of G4 (black) and G4A (red), with the in situ selected stars (dotted lines) and accreted stars (dashed lines). The vertical bars indicate the position of the radius of half-mass for the different components. The half-mass radius of the accreted component is larger than the half-mass radius of the in situ component. As the accreted material dominates the stellar density profiles at smaller radii when AGN feedback is turned on, the half-mass radius of the total stellar mass (in situ + accreted) increases.

well, and can smooth the density profiles of both stars and DM in the most central parts (Mashchenko, Couchman & Wadsley 2006; Peirani, Kay & Silk 2008; Pontzen & Governato 2012; Teyssier et al. 2013), in conjunction with the adiabatic expansion of DM and stars (Blumenthal et al. 1986; Gnedin & Zhao 2002; Gnedin et al. 2004) produced by the decrease of the gas density due to AGN feedback in the centre of DM haloes. This effect can increase the size of galaxies and DM halo cores, but depends on the details of the accretion history on to the central galaxy (Martizzi, Teyssier & Moore 2013). Some of the galaxies show a larger in situ effective

radius in the AGN case compared to the no AGN case at high redshift where the wet and chaotic accretion takes place. This can trigger strong bursts of AGN feedback that may be effective at flattening the density profiles by star formation quenching. Also, we observe such flattening in the total mass density profiles (and in the DM component) and we will discuss this further in the next section by comparing our results from simulations to observations.

The fraction of cold gas within galaxies, $f_{\text{gas}} = M_{\text{ISM}} / (M_s + M_{\text{ISM}})$ (where M_{ISM} is the cold gas with gas density $n > n_0$ and within the galactic radius), both in central galaxy and in satellites ($M_{\text{ISM},s} = \sum_i M_{\text{ISM},s}^i$ summed over all satellites within the virial radius of the main halo), is declining with time with a gas fraction close to 0.1 for the no AGN case and 0.025 in the AGN case at $z = 0$ (Fig. 16). The gas fractions are much larger for high-redshift galaxies with values above 0.5, which are gas-dominated galaxies at $z = 4$. Thus, mergers between galaxies at high redshift are dissipative (wet), and are essentially dissipationless (dry) at low redshift. The presence of AGN feedback leads to a mild variation on the gas fraction of galaxies at $z < 2-3$, but even for runs including AGN feedback, galaxies above $z > 3$ are still gas-dominated systems. It confirms that AGN feedback exacerbates the effect of accretion of satellites on the effective radius at low redshift. As AGN feedback reduces the gas fraction within galaxies at low redshift, dry mergers become more efficient at puffing up the size of galaxies. However, at high redshift, the gas fraction between the AGN and no AGN runs are not very different, and it is the subsequent AGN activity that increases the effective radius of the, then, dominant in situ component (Fig. 13), by blowing gas away from galaxies (see Fig. 15).

3.3 Implications for galaxy scaling relations and mass distribution

The scaling relations between mass and kinematics can put strong constraints on the modelling of the population of massive galaxies. In Fig. 17, we show the relations between the effective radius r_{eff} and the stellar mass of the central galaxy at different redshifts. Independently of the adopted IMF, all galaxies simulated without AGN feedback lie below the $r_{\text{eff}}-M_s$ observational relation at $z = 0.2$ from the SLACS data (Auger et al. 2010a) that consists of ETGs within the mass range $10^{11} \lesssim M_s \lesssim 6 \times 10^{11} M_{\odot}$. These galaxies, suffering from over-cooling and being too massive, are also too compact. This increased compactness is expected if the amount of in situ star formation is too large, as the in situ formed stars have small effective radius compared to the effective radius of the accreted stellar distribution (Fig. 15).

The presence of AGN feedback increases the effective radius, while at the same time it reduces stellar masses and greatly improves the agreement between the simulations and observations for the four most massive galaxies (G3A, G4A, G5A, G6A). The simulation points with AGN feedback stand close to the observational result for the four most massive galaxies at $z = 0.2$, within the 2σ error bars (for a Chabrier IMF). If a Salpeter IMF is assumed, the AGN size-mass points of the four most massive galaxies at $z = 0.2$ stand within the 5σ relation. The two least massive galaxies are largely above the observational relation, which makes these galaxies too puffy. Such galaxies exist but are rare objects in the real Universe (Williams et al. 2010). It is difficult to explain this particular behaviour, but one should note as they are the lightest galaxies, they are also the galaxies that are the most affected by the finite resolution. At redshift $z = 2$, the effective radius of these galaxies is very close to the resolution limit of the grid ($r_{\text{eff}} \simeq 2$ kpc against a $\Delta x = 0.5$ kpc resolution), and the galaxy gets extra support against gravity from

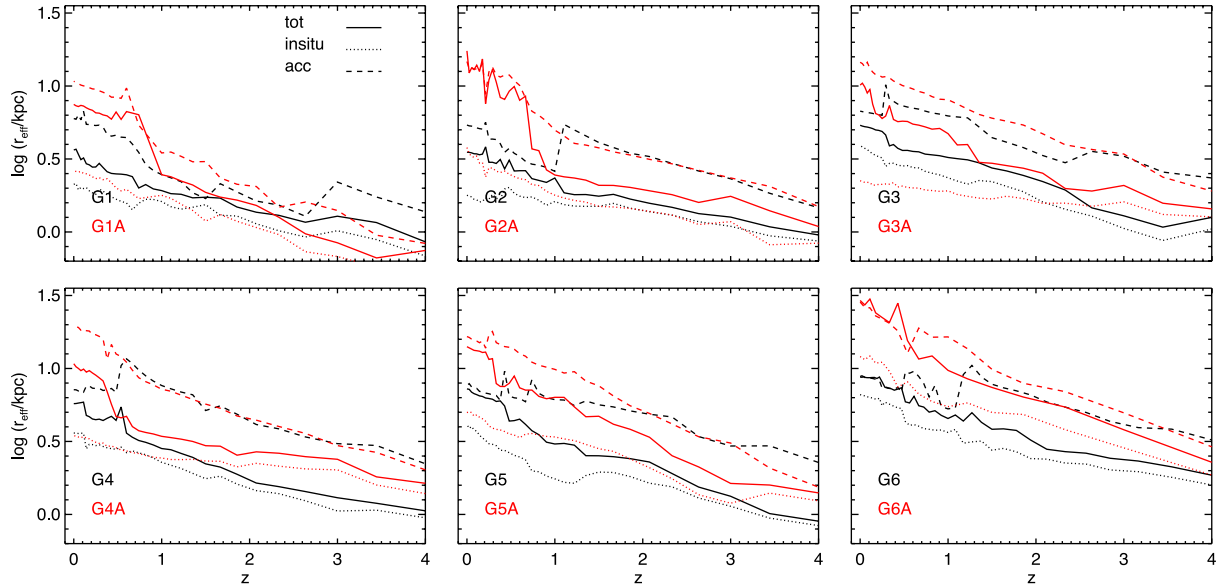


Figure 15. Effective radius of the central galaxy (solid), of the in situ component only (dotted) and of the accreted component only (dashed) as a function of redshift for the simulations GX without AGN feedback (black) or GXA with AGN feedback (red). All galaxies including AGN feedback show an increased value of the effective radius relative to the no AGN case.

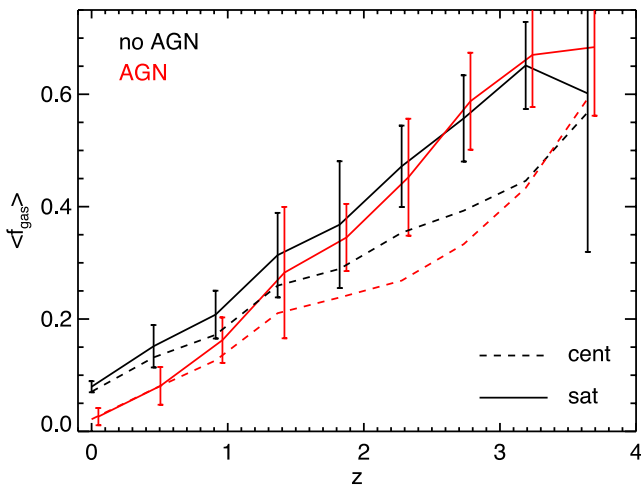


Figure 16. Average gas fraction as a function of redshift in the satellites (solid lines) and in the central galaxy (dashed lines) of the six simulated haloes with (red) or without (black) AGN feedback, with the standard deviation (error bars). Galaxies are more gas-poor at low redshift than at high redshift and AGN feedback reduces further the fraction of cold gas.

the finite cell size. At even higher redshifts, this effect is true for all simulated galaxies as they are smaller, and could have some non-negligible effects on the final size–mass relation at $z = 0$.

Galaxies are evolving in size with time while they accumulate stars (Fig. 15), and there is a small variation of the size–mass relation with redshift for the AGN feedback simulations, with galaxies being more compact at high redshift (i.e. the distribution of r_{eff} versus M_s at high redshift is below this relation at low redshift; Fig. 17). Observations suggest such an evolution with time in the compactness of galaxies (Trujillo et al. 2007; Cimatti et al. 2008; Saracco, Longhetti & Andreon 2009; van Dokkum et al. 2010; Huertas-Company et al. 2013), and the effective radius is of the order of $\sim 1.5 - 2$ smaller at redshift 1 than at redshift 0 at constant mass for ETGs (Huertas-Company et al. 2013). On the opposite,

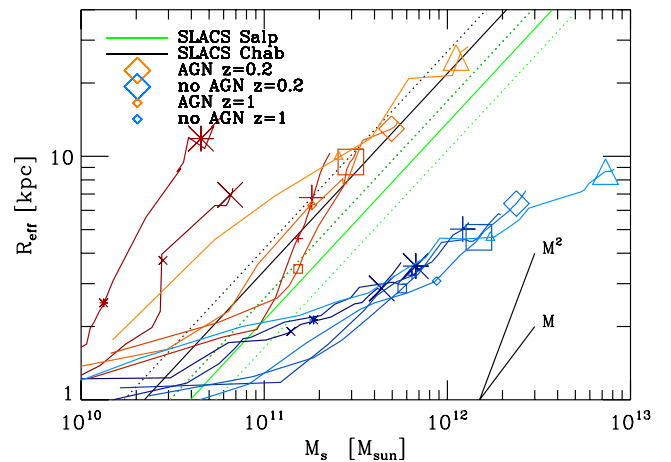


Figure 17. Effective radius r_{eff} versus stellar mass M_s for our six haloes G1 (crosses), G2 (stars), G3 (pluses), G4 (squares), G5 (diamonds) and G6 (triangles) with (red) or without (blue) AGN feedback computed at different redshifts: $z = 0.2$ are large symbols and $z = 1$ are small symbols. The observed relations from the SLACS (at $z \sim 0.2$) are overplotted as solid lines with their 2σ standard deviation (dot) assuming either a Chabrier (black), or a Salpeter IMF (green). Galaxies simulated with AGN feedback are less compact than those simulated without AGN feedback, and are more compact at high redshift than they are at low redshift.

simulation points without AGN feedback show the opposite trend: galaxies tend to be less compact at high redshift. From virial theorem arguments, it can be shown that galaxy growth driven by minor mergers should follow $r_{\text{eff}} \propto M_s^2$ and $r_{\text{eff}} \propto M_s$ through major mergers (see Hilz et al. 2012). For the AGN runs, mergers drive the size growth of the central galaxies, both minor and major. This leads to an intermediate relation $M_s - M_s^2$. However for the no AGN simulations, we clearly see that the size growth follows a shallower change with mass. This can be explained by the fact that these galaxies are dominated by the in situ star formation that concentrates stars in the innermost parts of the galaxies where the cold gas is deposited.

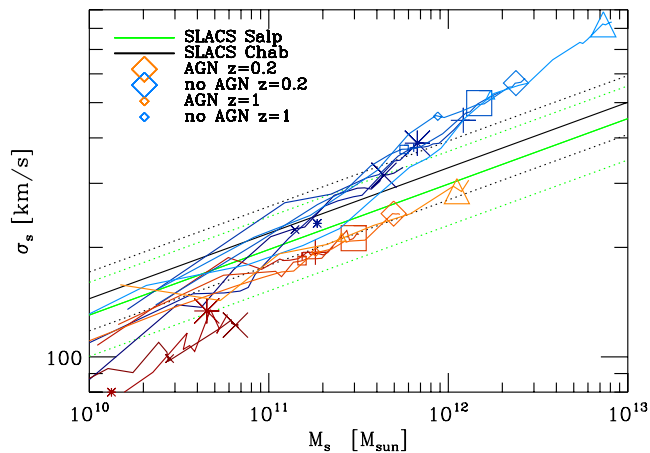


Figure 18. Same as Fig. 17 for the velocity dispersion of stars σ_s within $r_{\text{eff}}/2$ versus stellar mass M_s . Galaxies simulated with AGN feedback have lower velocity dispersion values than for galaxies simulated without AGN feedback.

Note that there is likely an effect of limited resolution on the size evolution, that more importantly impacts the low-mass galaxies in their early stages (see the flattening of the curves at $z > 1$ in Fig. 17). Because of additional numerical support we can expect their size to be artificially increased when they are close to the resolution limit.

We also measured the projected velocity dispersion of stars σ_s within $r_{\text{eff}}/2$ relative to their galaxy mass M_s (Fig. 18). The galaxies without AGN feedback show large values of σ_s . This is the direct consequence of the size–mass relation: more compact galaxies need more dynamical support (velocity dispersion). At $z = 0.2$ the four most massive galaxies without AGN lie above 2σ of the observational relation, while the two least massive lie within the relation (for a Chabrier IMF). As can be predicted from the size–mass relation, the presence of AGN feedback produces more extended galaxies and, thus, galaxies with lower values of stellar velocity dispersion. The four most massive galaxies with AGN have values of $\sigma_s - M_s$ in better agreement with observations than in the absence of AGN. As for the size–mass relation, the $\sigma_s - M_s$ points for the two least massive galaxies are at more than 2σ away from the observational relation at $z = 0.2$ if AGN feedback is incorporated. These low-mass ETGs are above the size–mass observational fit and since they need less kinematic support because they are too extended, they lie below the velocity dispersion–mass observational law.

An even more stringent observational constraint to reproduce is the Fundamental Plane of ETGs. Here, we measure the mass equivalent, namely the M_s -plane (Bolton et al. 2007, 2008; Auger et al. 2010), that links the galaxy size to the galaxy mass and velocity dispersion (Fig. 19). All galaxies simulated without AGN feedback stand above the M_s -plane. For the AGN feedback simulations, we find that the four most massive galaxies stand closer to the M_s -plane than in the case without AGN feedback and they favour a Chabrier IMF. For the two least massive galaxies including AGN, they stand below the M_s -plane, with the G2A galaxy being at more than 10σ away.

The slope of the total mass density profile measured by strong lensing provides a value close to isothermal $\gamma = -2.078$ ($\rho_{\text{tot}} \propto r^\gamma$) at $z = 0.2$ for ETGs (Koopmans et al. 2009; Auger et al. 2010; Barnabè et al. 2011). We measure the slope in our simulations for the average total density within a radius r such that $\rho_{\text{tot}} = M_{\text{tot}}(< r)/(4/3\pi r^3)$. We use two points to measure the average slope, at $r_{\text{eff}}/2$ and r_{eff} . The first striking result is that the measured slopes

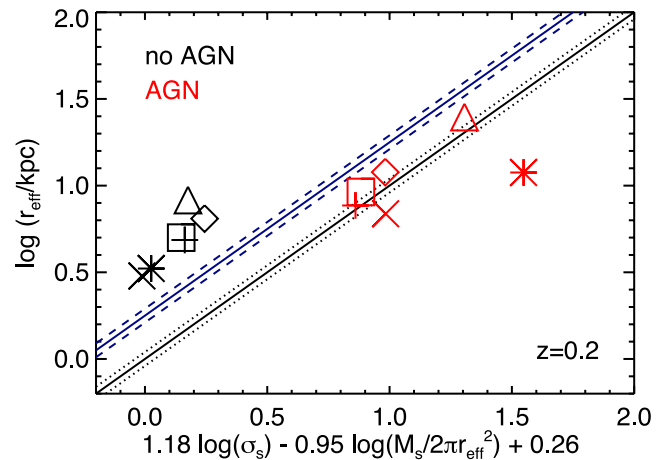


Figure 19. Stellar mass M_s -plane at $z = 0.2$ for galaxies with AGN feedback (red) and galaxies without AGN feedback (black). The observed relations from the SLACS (at $z \sim 0.2$) are overplotted as solid lines with their 2σ standard deviation (dot) assuming either a Chabrier (black), or a Salpeter IMF (blue). Galaxies simulated without AGN feedback lie above the M_s -plane, while galaxies with AGN feedback are closer to M_s -plane (favouring a Chabrier IMF).

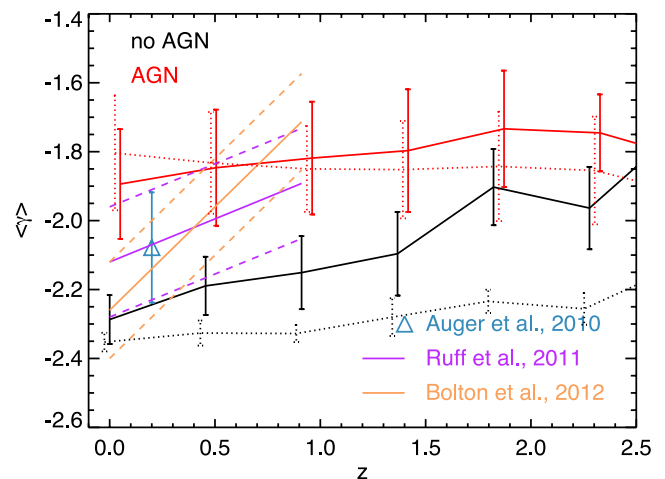


Figure 20. Average slope of the total mass density profile as a function of redshift for the six haloes with (red) or without (black) AGN feedback. The slope are measured between $r_{\text{eff}}/2$ and r_{eff} on the average mass density within radius r (solid lines) similar to observations, or between $2\Delta x$ and $0.1r_{\text{vir}}$ (dotted lines). Error bars correspond to the standard deviation. Observations from the SLACS sample (Auger et al. 2010a) at $z = 0.2$ are plotted in cyan. The observational trend of the slope with redshift found by Ruff et al. (2011) and Bolton et al. (2012) is plotted in violet and orange, respectively, with their intrinsic scatter. AGN feedback flattens the total density profiles. AGN feedback produces shallower total density profiles within galaxies.

are quite similar to runs with or without AGN, and are close to isothermal (see Fig. 20). At $z = 0$, galaxies without AGN feedback show an average slope close to $\gamma = -2.29 \pm 0.07$, while for the galaxies with AGN feedback profiles are flatter with $\gamma = -1.89 \pm 0.16$. Note that the measured scatter in the AGN feedback case is in good agreement with that found in the observations. As seen in Fig. 14, stellar density profiles are steeper than isothermal for the G4 and G4A haloes (but this is true for all zoomed haloes). Thus, DM populates preferentially the outer part of the galaxy, so that the total density profiles flatten up to γ above -2 for the AGN case. The difference in the value of the slope already happens at

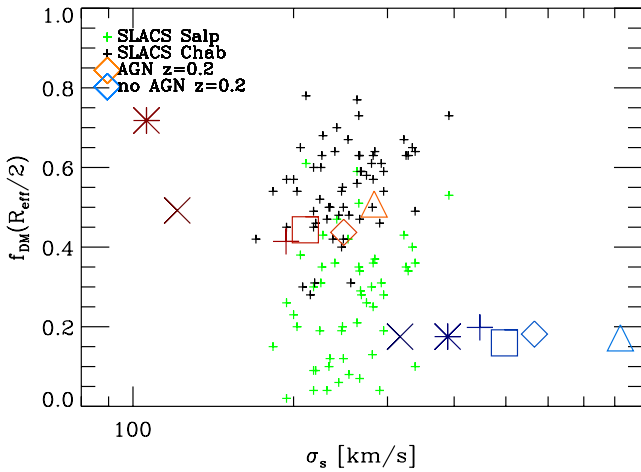


Figure 21. Same as Fig. 17 for the DM fraction f_{DM} within $r_{\text{eff}}/2$ versus the velocity dispersion of stars σ_s . Galaxies simulated with AGN feedback have larger DM fraction within $r_{\text{eff}}/2$ than galaxies simulated without AGN feedback.

$z = 2$.¹ Thus, AGN feedback at $z = 2$ has been able to significantly change the total distribution of matter. Note that the observational points stand between the values of the runs with and without AGN feedback, and that the error bars are compatible with both values. We also measure the slope between $2\Delta x$ and $0.1r_{\text{vir}}$, two points that are not affected by the presence of feedback, to clearly assess that the change in the slope is real and not just an effect of changing r_{eff} through feedback. The slope within $0.1r_{\text{vir}}$ shows the same features than the slope measured at r_{eff} : AGN feedback flattens the total mass density profile.

Combining strong lensing data at higher redshift, Ruff et al. (2011) and Bolton et al. (2012) provide an estimation of the variation of the slope γ with redshift. They find that the slope is steeper at low redshift than it is at high redshift, with a variation of 0.25 in Ruff et al. (2011) and 0.60 in Bolton et al. (2012) with redshift. Our simulations show such a mild evolution in the slope of the total density profile with redshift, and our measured averaged slope at high redshift $z \simeq 0.5$ –1 is in better agreement with observations for the AGN feedback runs. Cosmological simulations from Remus et al. (2013) show that massive ellipticals evolve towards profiles with $\gamma = -2$ slope at $z = 0$ due to a combination of dry minor and major mergers; however they find a steeper profile at high redshift which is at odds with our findings and with the observations.

Likewise, when comparing in Fig. 21, the projected DM fraction within half the effective radius at $z \sim 0.2$ in the SLACS data (Gavazzi et al. 2007; Auger et al. 2010a) and in our simulations, we find a better agreement for the simulation with AGN feedback turned on ($f_{\text{dm}} \sim 0.5$) than without ($f_{\text{dm}} \sim 0.2$), mostly because the stellar mass (or equivalently the velocity dispersion) without AGN feedback is too large. In the former case, the dark matter fraction is slightly more consistent with observations assuming a Chabrier IMF.

4 COMPARISON WITH PREVIOUS WORK

A key point of our work is that, in the absence of AGN feedback, the galaxies always exhibit a late-type morphology with a large disc

of stars as can be observed in the synthetic images in Fig. 6. We find similar results to Lackner et al. (2012) who use the ENZO (AMR code) to simulate some overdense and underdense regions of the universe: their stellar conversion efficiency is high $f_{\text{conv}} = 0.6$, and their most massive galaxies $M_s > 10^{12} M_{\odot}$ are dominated by in situ star formation $f_{\text{in situ}} = 60$ per cent at $z = 0$. They use similar physics (gas cooling, low efficiency star formation, SNe feedback and metal cooling) as for our simulations without AGN feedback. In the work from Oser et al. (2010) (see also Naab et al. 2007, 2009; Johansson, Naab & Ostriker 2012; Oser et al. 2012), they employ the GADGET code (Springel 2005) based on SPH, to study the formation of elliptical galaxies in group environments. The same basic physical ingredients as for our simulations without AGN, and in Lackner et al. (2012), are used in their work, except they use a larger value of the star formation efficiency $\epsilon_* \simeq 0.1$. However the results of Oser et al. (2010) are radically different from ours (and thus from Lackner et al. 2012): they naturally obtain elliptical galaxies with low stellar conversion efficiency $0.1 < f_{\text{conv}} < 0.45$, respectively, for high-mass and low-mass haloes in the mass range $10^{12} < M_h < 2.5 \times 10^{13} M_{\odot}$, and the growth of galaxies is largely dominated by the accretion of satellites with $f_{\text{in situ}} = 20$ per cent at $z = 0$ for the halo mass range corresponding to ours. Note that in SPH simulations of $M_h = 3 \times 10^{12} M_{\odot}$ halo by Khalatyan et al. (2008) using SPH, they find little difference in their galaxy mass and morphology between the AGN case and the no-AGN case at $z = 0$. The galaxy is more red with AGN feedback, and has a larger value of the Sérsic index, but the galaxy is an elliptical in both cases and has the same low stellar conversion efficiency $f_{\text{conv}} \simeq 0.2$ at $z = 0$.

There are several potential interpretations that can explain this difference in the results. The first one is that the high star formation efficiency adopted can account for the difference seen in the accreted versus in situ star formation. Higher efficiencies tend to form stars at higher redshift by rapidly converting gas into stars, thus, the fraction of accreted mass should increase at low redshift. We make that simple test by running the G1 and G2 simulations with a $\epsilon_* = 0.1$ efficiency (still without AGN feedback), and we found that the accreted fraction of the stellar mass has increased. In line with the analysis performed by the decomposition of in situ versus accreted origin of stars, we indeed find that the galaxy becomes more spherical (supported by the velocity dispersion of stars as opposed to rotation). However, the stellar mass obtained at $z = 0$ is the same ($M_s = 5.4 \times 10^{11} M_{\odot}$, $f_{\text{conv}} = 0.76$ for G1; and $M_s = 7.0 \times 10^{11} M_{\odot}$, $f_{\text{conv}} = 0.66$ for G2) as for the low star formation efficiency case ($M_s = 5.6 \times 10^{11} M_{\odot}$, $f_{\text{conv}} = 0.79$ for G1; and $M_s = 7.3 \times 10^{11} M_{\odot}$, $f_{\text{conv}} = 0.70$ for G2), and cannot account for the difference observed with Oser et al. (2010) ($f_{\text{conv}} \simeq 0.2$ for halo masses $M_h \simeq 6 \times 10^{12} M_{\odot}$). We observe that both DM mass resolution and spatial resolution are of comparable values in Oser et al. (2010) and here, even though it is difficult to compare a smoothing length with a minimum cell size.

Another much more worrying aspect is the different behaviour of AMR and SPH codes as already underlined by Scannapieco et al. (2012) for Milky Way haloes, and then by Vogelsberger et al. (2012) who compared results from the AREPO code (moving mesh Springel 2010) with GADGET in a statistical sense. With relatively similar physics, AMR codes (or moving mesh codes) tend to naturally produce overly massive disc-like galaxies, while SPH codes predict less massive galaxies that have already early-type shapes. This is in line with our findings: the ‘usual’ modelling of galaxy formation (i.e. not accounting for AGN feedback) with the RAMSES code leads to overly massive disc-like galaxies even in the centres of massive

¹ Above this redshift the value of $r_{\text{eff}}/2$ is too close to the resolution limit to be conclusive for the mass density slope.

groups of galaxies. This is potentially driven by a more accurate treatment of the gas instabilities in grid-based codes as demonstrated by Agertz et al. (2007). It can have critical consequences on the amount of gas mixing between satellites (cold phase) and the hot ambient medium in massive haloes which can lead to more efficient gas cooling (Sijacki et al. 2012). Moreover, the treatment of blast wave explosions (SN or AGN) with thin discontinuities can have problematic behaviours if the adaptive time-stepping becomes too aggressive (Durier & Dalla Vecchia 2012).

A careful inspection of the numerical treatment of the hydrodynamics and its consequences for the formation of massive galaxies remain to be conducted. This is especially important as it can lead to an underestimate of the role played by AGN feedback in shaping the masses, colours and morphologies of massive ETGs. We reserve this numerical comparison for future work.

Using a different technique, semi-analytical models of galaxy formation have also produced predictions for the amount of in situ versus accreted stellar material in massive galaxies. Hirschmann et al. (2012) show that AGN feedback plays an important role in reducing the fraction of in situ formed stars down to $f_{\text{in situ}} \simeq 0.5$ at $z = 0$ for the most massive galaxies equivalent to the mass range probed in this work, while this fraction goes up to $f_{\text{in situ}} \simeq 0.65\text{--}0.75$ in the absence of AGN feedback. Lee & Yi (2013) find even lower values of $f_{\text{in situ}} \simeq 0.2$ using their semi-analytical model with AGN feedback, while they obtain $f_{\text{in situ}} \simeq 0.7$ if no AGN feedback is considered (private communication with the authors). In both cases, the absence of AGN feedback leads to in situ-dominated galaxies with levels similar to what we find in our hydrodynamical simulations (as in Lackner et al. 2012). However, they find different values of the in situ fraction of stars for their semi-analytical models including AGN feedback, possibly because of the different implementations of AGN feedback.

5 CONCLUSION AND DISCUSSION

By means of high-resolution hydrodynamical cosmological simulations, we have studied the impact of AGN feedback on the formation and evolution of massive galaxies in the centre of groups of galaxies. The main finding of this work is that we have demonstrated that AGN feedback can turn blue massive late-type disc galaxies into red ETGs. This process happens because AGN feedback reduces the in situ star formation in the central most massive galaxy, and turns it into a stellar accretion-dominated system. In more detail, we find the following.

(i) The conversion efficiency of baryons into stars in the central galaxy is reduced by a factor of 7 from $f_{\text{conv}} = 0.7$ to $f_{\text{conv}} = 0.1$ at $z = 0$ due to AGN feedback.

(ii) Galaxies are intrinsically redder with AGN feedback than without, with, respectively, $g - r = 0.65$ and $g - r = 0.45$.

(iii) The DM mass fraction is increased (from $\langle f_{\text{DM}} \rangle = 0.53$ to $\langle f_{\text{DM}} \rangle = 0.83$) with AGN at $z = 0$, and stellar (from $\langle f_{\text{s}} \rangle = 0.42$ to $\langle f_{\text{s}} \rangle = 0.15$) and gas (from $\langle f_{\text{g}} \rangle = 0.04$ to $\langle f_{\text{g}} \rangle = 0.016$) fractions are reduced within the core of haloes (in $0.1r_{\text{vir}}$) at $z = 0$ by the presence of AGN feedback.

(iv) Central galaxies are rotation-dominated (discs with $v/\sigma > 1$) without AGN feedback, and dispersion-dominated (ellipticals with $v/\sigma < 1$) with AGN feedback.

(v) The fraction of stellar mass in the halo locked into satellites is larger if AGN feedback is present. It leads to the formation of central ETGs dominated by accretion of stars rather than by in situ star formation at $z = 0$.

(vi) Galaxies are dominated by in situ star formation at high redshift because they are gas-rich systems that rapidly convert gas into stars. As their reservoir of gas decreases with time and the SFR is quenched, the proportion of accreted mass increases.

(vii) Accreted stars are deposited far away from the central galaxy, while in situ formed stars are close to the centre of the halo. As a consequence, the effective radius of the accreted distribution of stars is larger than that of the in situ component.

(viii) Because of the increased fraction of accreted material in the AGN simulations and the enhanced dissipationless nature of low-redshift mergers, the effective radius of central galaxies is larger, and galaxies are less compact.

(ix) The presence of AGN feedback provides a better fit to the observed dynamical scaling relations (size–mass, velocity–mass, M_{s} –plane) than without AGN feedback.

(x) With AGN feedback, galaxies are smaller at high redshift at constant mass, while they are larger without AGN feedback.

(xi) The total mass density profiles in galaxies are affected by AGN feedback, and they get shallower.

We note finally that the conclusions of this work could be mitigated by some possible artefacts of our methodology. We employ a finite cell size resolution of 0.5 kpc, which can possibly affect the compactness of the simulated galaxies in particular at high redshift, where their sizes approach the resolution limit. The stellar–halo mass relation at $z = 0$ is compatible with a Salpeter IMF for the most massive galaxies and with a Kroupa (or Chabrier) IMF for the least massive galaxies. In contrast, the size–mass relation favours a Kroupa IMF for the most massive galaxies, while the two least massive ones are excluded from the observational constraints (Kroupa or Salpeter). This leads to an inconsistency that can be the outcome of a lack of resolution, or wrong/missing modelling of the galactic physics, that remains to be explored further. As the multiphase structure of the gas is not resolved, the formation of massive clumps of gas produced by the disc instabilities at high redshift is not triggered (Ageret, Teyssier & Moore 2009; Dekel, Sari & Ceverino 2009) and any morphological quenching associated with this phenomenon is missed (Martig et al. 2009). However, the increase in resolution is not enough to prevent the galaxies from being too massive and strong feedback processes are still required (Dubois et al. 2013). Also, because of finite computational time, we limited our sample to six objects over one dynamical range of halo mass. More haloes spanning a broader mass range have to be simulated to obtain better statistical significance on our preliminary theoretical predictions in terms of both mean average trends and intrinsic scatter. We stress that, without AGN feedback, *none* of the observational constraints can be reproduced regardless of the choice of the IMF.

As already highlighted by many authors (e.g. Boylan-Kolchin et al. 2006; Khochfar & Silk 2006b; Maller et al. 2006; Naab et al. 2006, 2007; Bournaud et al. 2007; De Lucia & Blaizot 2007; Guo & White 2008; Hopkins et al. 2009; Nipoti et al. 2009; Feldmann et al. 2010; Shankar et al. 2013, and references therein), the role of the mergers of central galaxies with their satellites, and particularly of dry mergers, is crucial to understanding the size and velocity dispersion of galaxies and their evolution with time. We intentionally did not discuss in details the singular role of minor versus major mergers, or wet versus dry mergers, but instead we emphasized the particular effects of AGN feedback in transforming in situ dominated galaxies into accretion-dominated systems. However, we note that dry mergers become increasingly more dominant at low redshift, driving the low-redshift evolution of galaxy sizes, and that AGN feedback enhances this effect further. In future work we will

perform a dedicated study of these effects by employing a more statistically significant sample of galaxies.

Finally, when comparing our results, without AGN feedback, to the existing literature employing hydrodynamical cosmological simulations and the formation of ETGs (mostly without using AGN feedback), we found our results to be consistent with galaxies simulated with an AMR technique (blue massive discs dominated by in situ star formation), and inconsistent with those obtained with SPH (red ellipticals dominated by accretion). This conflict calls for a thorough analysis of the respective merits of the different numerical techniques and their consequences for the formation and evolution of massive galaxies.

ACKNOWLEDGEMENTS

We are grateful to Julien Devriendt, Christophe Pichon, Francesco Shankar, Romain Teyssier and Tommaso Treu for stimulating discussions. We thank the anonymous referee for his useful comments that improved the quality of the paper. The simulations presented here were run on the DiRAC facility jointly funded by STFC, the Large Facilities Capital Fund of BIS and the University of Oxford. This research is part of the Horizon-UK project. This research was supported in part by ERC project 267117 (DARK) hosted by Université Pierre et Marie Curie - Paris 6. RG acknowledges the CNES for its financial support and the PNCG for support in the organization of a workshop on ETGs in Paris, July 2012. YD acknowledges Fabio Acero and Stéphanie Gain for the hospitality provided during the redaction of this paper.

REFERENCES

- Agertz O. et al., 2007, *MNRAS*, 380, 963
 Agertz O., Teyssier R., Moore B., 2009, *MNRAS*, 397, L64
 Aubert D., Pichon C., Colombi S., 2004, *MNRAS*, 352, 376
 Auger M. W., Treu T., Bolton A. S., Gavazzi R., Koopmans L. V. E., Marshall P. J., Moustakas L. A., Burles S., 2010a, *ApJ*, 724, 511
 Auger M. W., Treu T., Gavazzi R., Bolton A. S., Koopmans L. V. E., Marshall P. J., 2010b, *ApJ*, 721, L163
 Barnabè M., Czoske O., Koopmans L. V. E., Treu T., Bolton A. S., 2011, *MNRAS*, 415, 2215
 Bate M. R., Bonnell I. A., Price N. M., 1995, *MNRAS*, 277, 362
 Bernardi M., Sheth R. K., Nichol R. C., Schneider D. P., Brinkmann J., 2005, *AJ*, 129, 61
 Birnboim Y., Dekel A., 2003, *MNRAS*, 345, 349
 Blumenthal G. R., Faber S. M., Flores R., Primack J. R., 1986, *ApJ*, 301, 27
 Boehringer H., Voges W., Fabian A. C., Edge A. C., Neumann D. M., 1993, *MNRAS*, 264, L25
 Bolton A. S., Burles S., Treu T., Koopmans L. V. E., Moustakas L. A., 2007, *ApJ*, 665, L105
 Bolton A. S., Treu T., Koopmans L. V. E., Gavazzi R., Moustakas L. A., Burles S., Schlegel D. J., Wayth R., 2008, *ApJ*, 684, 248
 Bolton A. S. et al., 2012, *ApJ*, 757, 82
 Bondi H., 1952, *MNRAS*, 112, 195
 Booth C. M., Schaye J., 2009, *MNRAS*, 398, 53
 Bournaud F., Jog C. J., Combes F., 2007, *A&A*, 476, 1179
 Bower R. G., Benson A. J., Malbon R., Helly J. C., Frenk C. S., Baugh C. M., Cole S., Lacey C. G., 2006, *MNRAS*, 370, 645
 Boylan-Kolchin M., Ma C.-P., Quataert E., 2006, *MNRAS*, 369, 1081
 Bundy K., Fukugita M., Ellis R. S., Targett T. A., Belli S., Kodama T., 2009, *ApJ*, 697, 1369
 Cappellari M. et al., 2013, *MNRAS*, 432, 1862
 Cattaneo A., Dekel A., Devriendt J., Guiderdoni B., Blaizot J., 2006, *MNRAS*, 370, 1651
 Chabrier G., 2003, *PASP*, 115, 763
 Chapon D., Mayer L., Teyssier R., 2013, *MNRAS*, 429, 3114
 Chartas G., Brandt W. N., Gallagher S. C., 2003, *ApJ*, 595, 85
 Cimatti A. et al., 2008, *A&A*, 482, 21
 Conroy C., van Dokkum P. G., 2012, *ApJ*, 760, 71
 Conselice C. J., Mortlock A., Bluck A. F. L., Grützbauch R., Duncan K., 2013, *MNRAS*, 430, 1051
 Croton D. J. et al., 2006, *MNRAS*, 365, 11
 Daddi E. et al., 2005, *ApJ*, 626, 680
 Daddi E. et al., 2010, *ApJ*, 713, 686
 De Lucia G., Blaizot J., 2007, *MNRAS*, 375, 2
 Dekel A. et al., 2009a, *Nat*, 457, 451
 Dekel A., Sari R., Ceverino D., 2009b, *ApJ*, 703, 785
 Di Matteo T., Colberg J., Springel V., Hernquist L., Sijacki D., 2008, *ApJ*, 676, 33
 Dubois Y., Teyssier R., 2008, *A&A*, 477, 79
 Dubois Y., Devriendt J., Slyz A., Teyssier R., 2010, *MNRAS*, 409, 895
 Dubois Y., Devriendt J., Teyssier R., Slyz A., 2011, *MNRAS*, 417, 1853
 Dubois Y., Devriendt J., Slyz A., Teyssier R., 2012, *MNRAS*, 420, 2662
 Dubois Y., Pichon C., Devriendt J., Silk J., Haehnelt M., Kimm T., Slyz A., 2013, *MNRAS*, 428, 2885
 Durier F., Dalla Vecchia C., 2012, *MNRAS*, 419, 465
 Feldmann R., Carollo C. M., Mayer L., Renzini A., Lake G., Quinn T., Stinson G. S., Yepes G., 2010, *ApJ*, 709, 218
 Few C. G., Gibson B. K., Courty S., Michel-Dansac L., Brook C. B., Stinson G. S., 2012, *A&A*, 547, A63
 Gavazzi R., Treu T., Rhodes J. D., Koopmans L. V. E., Bolton A. S., Burles S., Massey R. J., Moustakas L. A., 2007, *ApJ*, 667, 176
 Gnedin O. Y., Zhao H., 2002, *MNRAS*, 333, 299
 Gnedin O. Y., Kravtsov A. V., Klypin A. A., Nagai D., 2004, *ApJ*, 616, 16
 Graham A. W., Scott N., 2013, *ApJ*, 764, 151
 Grillo C., Gobat R., 2010, *MNRAS*, 402, L67
 Grillo C., Gobat R., Rosati P., Lombardi M., 2008, *A&A*, 477, L25
 Gültekin K. et al., 2009, *ApJ*, 698, 198
 Guo Q., White S. D. M., 2008, *MNRAS*, 384, 2
 Haardt F., Madau P., 1996, *ApJ*, 461, 20
 Häring N., Rix H.-W., 2004, *ApJ*, 604, L89
 Hilz M., Naab T., Ostriker J. P., Thomas J., Burkert A., Jesseit R., 2012, *MNRAS*, 425, 3119
 Hirschmann M., Naab T., Somerville R. S., Burkert A., Oser L., 2012, *MNRAS*, 419, 3200
 Hopkins P. F., Hernquist L., Cox T. J., Keres D., Wuyts S., 2009, *ApJ*, 691, 1424
 Huertas-Company M. et al., 2013, *MNRAS*, 428, 1715
 Johansson P. H., Naab T., Ostriker J. P., 2012, *ApJ*, 754, 115
 Kennicutt R. C., Jr, 1998, *ApJ*, 498, 541
 Kereš D., Katz N., Weinberg D. H., Davé R., 2005, *MNRAS*, 363, 2
 Khalatyan A., Cattaneo A., Schramm M., Gottlöber S., Steinmetz M., Wisotzki L., 2008, *MNRAS*, 387, 13
 Khochfar S., Silk J., 2006a, *ApJ*, 648, L21
 Khochfar S., Silk J., 2006b, *MNRAS*, 370, 902
 Kimm T. et al., 2012, *MNRAS*, 425, L96
 King I., 1962, *AJ*, 67, 471
 King A., 2003, *ApJ*, 596, L27
 Komatsu E. et al., 2011, *ApJS*, 192, 18
 Koopmans L. V. E. et al., 2009, *ApJ*, 703, L51
 Kroupa P., 2001, *MNRAS*, 322, 231
 Krumholz M. R., Tan J. C., 2007, *ApJ*, 654, 304
 Krumholz M. R., McKee C. F., Klein R. I., 2004, *ApJ*, 611, 399
 Lackner C. N., Ostriker J. P., 2010, *ApJ*, 712, 88
 Lackner C. N., Cen R., Ostriker J. P., Joung M. R., 2012, *MNRAS*, 425, 641
 Laporte C. F. P., White S. D. M., Naab T., Ruzsowski M., Springel V., 2012, *MNRAS*, 424, 747
 Lee J., Yi S. K., 2013, *ApJ*, 766, 38
 McCarthy I. G. et al., 2010, *MNRAS*, 406, 822
 McCarthy I. G., Schaye J., Bower R. G., Ponman T. J., Booth C. M., Dalla Vecchia C., Springel V., 2011, *MNRAS*, 412, 1965
 Magorrian J. et al., 1998, *AJ*, 115, 2285
 Maller A. H., Katz N., Kereš D., Davé R., Weinberg D. H., 2006, *ApJ*, 647, 763

- Martig M., Bournaud F., Teyssier R., Dekel A., 2009, *ApJ*, 707, 250
 Martizzi D., Teyssier R., Moore B., 2013, *MNRAS*, 432, 1947
 Mashchenko S., Couchman H. M. P., Wadsley J., 2006, *Nat*, 442, 539
 Moster B. P., Somerville R. S., Maubetsch C., van den Bosch F. C., Macciò A. V., Naab T., Oser L., 2010, *ApJ*, 710, 903
 Naab T., Khochfar S., Burkert A., 2006, *ApJ*, 636, L81
 Naab T., Johansson P. H., Ostriker J. P., Efstathiou G., 2007, *ApJ*, 658, 710
 Naab T., Johansson P. H., Ostriker J. P., 2009, *ApJ*, 699, L178
 Nipoti C., Treu T., Auger M. W., Bolton A. S., 2009, *ApJ*, 706, L86
 Ocvirk P., Pichon C., Teyssier R., 2008, *MNRAS*, 390, 1326
 Oser L., Ostriker J. P., Naab T., Johansson P. H., Burkert A., 2010, *ApJ*, 725, 2312
 Oser L., Naab T., Ostriker J. P., Johansson P. H., 2012, *ApJ*, 744, 63
 Ostriker E. C., 1999, *ApJ*, 513, 252
 Peirani S., Kay S., Silk J., 2008, *A&A*, 479, 123
 Peirani S., Crockett R. M., Geen S., Khochfar S., Kaviraj S., Silk J., 2010, *MNRAS*, 405, 2327
 Pontzen A., Governato F., 2012, *MNRAS*, 421, 3464
 Puchwein E., Sijacki D., Springel V., 2008, *ApJ*, 687, L53
 Rasera Y., Teyssier R., 2006, *A&A*, 445, 1
 Rees M. J., Ostriker J. P., 1977, *MNRAS*, 179, 541
 Remus R.-S., Burkert A., Dolag K., Johansson P. H., Naab T., Oser L., Thomas J., 2013, *ApJ*, 766, 71
 Ruff A. J., Gavazzi R., Marshall P. J., Treu T., Auger M. W., Brault F., 2011, *ApJ*, 727, 96
 Rusin D., Kochanek C. S., Keeton C. R., 2003, *ApJ*, 595, 29
 Salpeter E. E., 1955, *ApJ*, 121, 161
 Saracco P., Longhetti M., Andreon S., 2009, *MNRAS*, 392, 718
 Scannapieco C. et al., 2012, *MNRAS*, 423, 1726
 Shakura N. I., Sunyaev R. A., 1973, *A&A*, 24, 337
 Shankar F., Marulli F., Bernardi M., Mei S., Meert A., Vikram V., 2013, *MNRAS*, 428, 109
 Sijacki D., Springel V., 2006, *MNRAS*, 366, 397
 Sijacki D., Springel V., di Matteo T., Hernquist L., 2007, *MNRAS*, 380, 877
 Sijacki D., Vogelsberger M., Kereš D., Springel V., Hernquist L., 2012, *MNRAS*, 424, 2999
 Silk J., Rees M. J., 1998, *A&A*, 331, L1
 Somerville R. S., Hopkins P. F., Cox T. J., Robertson B. E., Hernquist L., 2008, *MNRAS*, 391, 481
 Sonnenfeld A., Treu T., Gavazzi R., Marshall P. J., Auger M. W., Suyu S. H., Koopmans L. V. E., Bolton A. S., 2012, *ApJ*, 752, 163
 Spiniello C., Koopmans L. V. E., Trager S. C., Czoske O., Treu T., 2011, *MNRAS*, 417, 3000
 Spiniello C., Trager S. C., Koopmans L. V. E., Chen Y. P., 2012, *ApJ*, 753, L32
 Springel V., 2005, *MNRAS*, 364, 1105
 Springel V., 2010, *MNRAS*, 401, 791
 Springel V., Hernquist L., 2003, *MNRAS*, 339, 289
 Sutherland R. S., Dopita M. A., 1993, *ApJS*, 88, 253
 Tacconi L. J. et al., 2010, *Nat*, 463, 781
 Teyssier R., 2002, *A&A*, 385, 337
 Teyssier R., Moore B., Martizzi D., Dubois Y., Mayer L., 2011, *MNRAS*, 414, 195
 Teyssier R., Pontzen A., Dubois Y., Read J. I., 2013, *MNRAS*, 429, 3068
 Thomas J. et al., 2011, *MNRAS*, 415, 545
 Toro E. F., Spruce M., Speares W., 1994, *Shock Waves*, 4, 25
 Tremaine S. et al., 2002, *ApJ*, 574, 740
 Treu T., Auger M. W., Koopmans L. V. E., Gavazzi R., Marshall P. J., Bolton A. S., 2010, *ApJ*, 709, 1195
 Truelove J. K., Klein R. I., McKee C. F., Holliman J. H., II, Howell L. H., Greenough J. A., 1997, *ApJ*, 489, L179
 Trujillo I. et al., 2006, *ApJ*, 650, 18
 Trujillo I., Conselice C. J., Bundy K., Cooper M. C., Eisenhardt P., Ellis R. S., 2007, *MNRAS*, 382, 109
 Tweed D., Devriendt J., Blaizot J., Colombi S., Slyz A., 2009, *A&A*, 506, 647
 van de Voort F., Schaye J., Booth C. M., Haas M. R., Dalla Vecchia C., 2011, *MNRAS*, 414, 2458
 van Dokkum P. G. et al., 2010, *ApJ*, 709, 1018
 Vogelsberger M., Sijacki D., Kereš D., Springel V., Hernquist L., 2012, *MNRAS*, 425, 3024
 White S. D. M., Frenk C. S., 1991, *ApJ*, 379, 52
 Williams R. J., Quadri R. F., Franx M., van Dokkum P., Toft S., Kriek M., Labbé I., 2010, *ApJ*, 713, 738
 Wyithe J. S. B., Loeb A., 2003, *ApJ*, 595, 614

This paper has been typeset from a $\text{\TeX}/\text{\LaTeX}$ file prepared by the author.